GENERALIZED DRAG LAW BASED ON RASEX AND FLIP DATA

final report

Grant No. N00014-96-1-0014

Larry Mahrt
College of Oceanic and Atmospheric Sciences
Oregon State University
Corvallis, OR 97331

Prepared for:

Scott Sandgathe
Atmospheric Modeling and Prediction
Office of Naval Research

1 December 1997

GENERALIZED DRAG LAW BASED ON RASEX AND FLIP DATA

final report

Grant No. N00014-96-1-0014

Larry Mahrt
College of Oceanic and Atmospheric Sciences
Oregon State University
Corvallis, OR 97331

Prepared for:

Scott Sandgathe
Atmospheric Modeling and Prediction
Office of Naval Research

1 December 1997

Generalized Drag Law Based on RASEX and FLIP Data

1. Introduction

The research supported by Grant N00014-1-96-0014 concentrated on formulating the drag coefficient and transfer coefficient for heat in the coastal zone using primarily 10 m data collected from an offshore instrumented mast during the Risø Air Sea Experiment (RASEX). This mast was located 2 km off of the Danish coast in 4 m of water. In "Fetch Limited Drag Coefficients" (Chapter 2), existing formulations of the surface roughness length and drag coefficient are evaluated. New formulations are recommended which better include the influence of wave state and fetch. In "Heat Flux in the Coastal Zone" (Chapter 3), the transfer coefficient for heat is found to be sensitive to the shallow depth of the internal boundary layer in offshore flow. As a result, existing parameterizations overestimate the heat flux by a factor of two. A new relationship is proposed for both the thermal roughness length and the transfer coefficient.

Preliminary work has been completed on evaluation of the universal profile functions (nondimensional wind shear and temperature gradient functions) briefly summarized in Chapter 4. Chapter 5 presents work from several miscellaneous studies.

2. FETCH LIMITED DRAG COEFFICIENTS

DEAN VICKERS and L. MAHRT
College of Oceanic and Atmospheric Sciences, Oregon State University, Corvallis, OR 97331, U.S.A.

(Received in final form 1 May, 1997)

Abstract. Measurements made at a tower located 2 km off the coast of Denmark in shallow water during the Risø Air Sea Experiment (RASEX) are analyzed to investigate the behaviour of the drag coefficient in the coastal zone. For a given wind speed, the drag coefficient is larger during conditions of short fetch (2-5 km) off-shore flow with younger growing waves than it is for longer fetch (15-25 km) on-shore flow. For the strongest on-shore winds, wave breaking enhances the drag coefficient.

Variation of the neutral drag coefficient in RASEX is dominated by variation of wave age, frequency bandwidth of the wave spectra and wind speed. The frequency bandwidth is proportional to the broadness of the wave height spectra and is largest during conditions of light wind speeds. Using the RASEX data, simple models of the drag coefficient and roughness length are developed in terms of wind speed, wave age and bandwidth. An off-shore flow model of the drag coefficient in terms of nondimensional fetch is developed for situations when the wave state is not known.

Key words: Surface drag, Drag laws, Sea surface stress, Wave age

1. Introduction

The rate of momentum transfer between the atmosphere and the ocean is proportional to the 'roughness' of the waves. Atmospheric wind speed and stability, and the size, shape and phase velocity of the locally wind-generated waves and swell all affect the wind stress. In coastal regions, the wind stress may also be related to bottom topography, shoaling waves and development of internal boundary layers with off-shore flow.

A common method of parameterizing the surface wind stress, τ, in atmospheric and oceanic models is by specification of a drag coefficient, C_d, in the bulk formula

$$\tau = \rho C_d U^2 \tag{1}$$

where U is the wind speed relative to the current and ρ is the air density.

Numerous investigators have documented greater wind stress over young and developing wave fields compared to older wave fields which are more in equilibrium with the wind (e.g., Kitaigorodskii, 1970; Snyder et al., 1981; Geernaert et al., 1987; Donelan, 1990; Smith et al., 1992; Donelan et al., 1993). Two mechanisms that could explain this stress dependence on wave age are: 1) younger waves travel with slower phase speed relative to the wind and thus provide greater bulk shear between the interface and atmospheric surface layer, and 2) younger waves are steeper, which can lead to enhanced flow separation from individual wave crests and stronger pressure drag. Younger developing waves occur with atmospheric flow

Boundary-Layer Meteorology **85:** 53–79, 1997.

acceleration (changing wind direction or speed), and with fetch limited off-shore flow. The wave steepness is also enhanced by shoaling as waves propagate into shallow water (Smith, 1980; Freilich and Guza, 1984; Freilich et al., 1990).

In this study we analyze off-shore tower measurements of wind speed, atmospheric stability, wind stress and wave height to examine the variability of the neutral 10 m drag coefficient. Our analysis will focus on simple model formulations of the drag coefficient which attempt to implicitly parameterize the complex processes affecting wind stress in the coastal zone.

The field data and data analysis methods are discussed in Section 2. The drag coefficient and wave state dependence on fetch, wind speed and nonstationarity are presented in Section 3. Simple models of the drag coefficient and roughness length for the coastal zone are presented in Section 4. Since wave state information is normally not available in numerical models, a new model is developed in Section 5 where wave state parameters are replaced by a nondimensional fetch parameter. Our conclusions are in Section 6.

2. Field data

The full RASEX experiment instrumentation is described in Barthelmie et al. (1994) and Højstrup et al. (1997). In this study, we consider observations taken at the sea mast west tower, located 2 km off the northwestern coast of the island of Lolland, Denmark, in 4 m of water, for the intensive observing period 3 October through 8 November 1994 (Figure 1). The variation in mean water depth due to tides is approximately 0.3 m. Local off-shore flow conditions are characterized by a sea fetch ranging between 2 km and 5 km and upstream water depth ranging from 0 m to 4 m. On-shore flow has a fetch between 15 km and 25 km and water depths from 4 m to 20 m. The nearby land surface is relatively flat.

Fast response (20 Hz) observations from a Gill/Solent Ultrasonic sonic anemometer with an asymmetric head positioned 10 m above the mean sea surface were used to calculate the wind speed, wind stress and the buoyancy flux. Flow distortion studies performed by J. Højstrup (Risø National Laboratory, Roskilde, Denmark; personal communication) indicate that the 10 m sonic measurements suffer the least flow distortion due to sonic design and mounting, and in this study we only include flux measurements from the 10 m sonic.

The virtual temperature fluctuations from the sonic anemometer were corrected to account for bending of the acoustic wave by cross-wind flow (Schotanus et al., 1983). A single set of tilt angles were used to correct for the tilt of the sonic anemometer (Mahrt et al., 1996). Wind directions between 340 and 120 degrees at the sea mast west location were discarded from the analysis because of potential upwind interference from the tower and an array of wind turbines northeast of the tower.

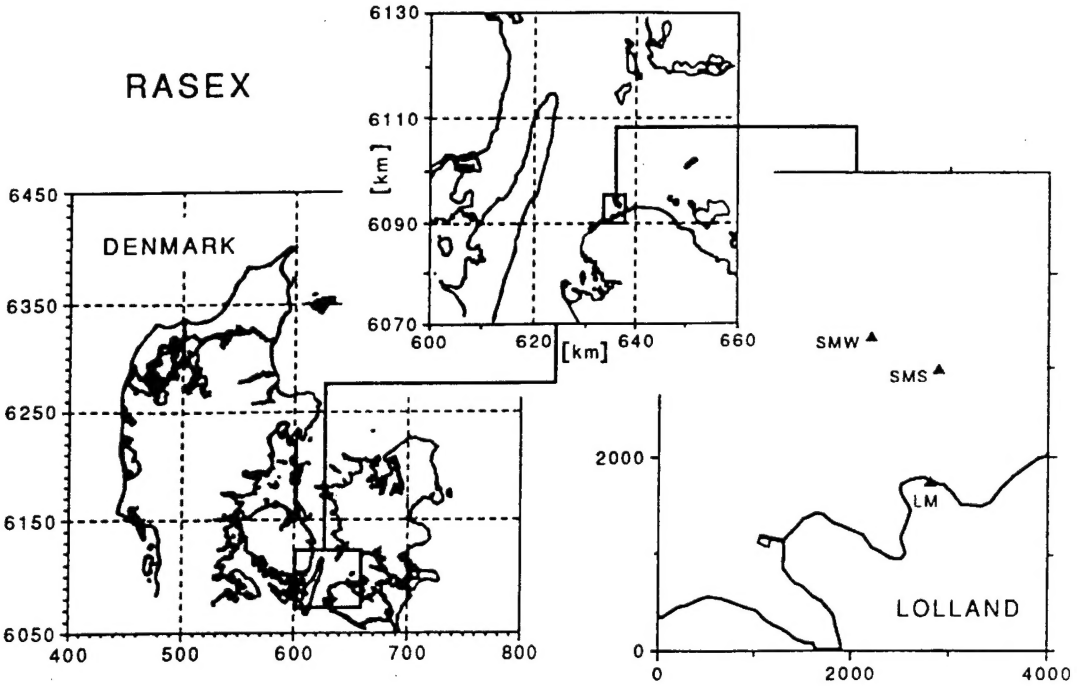

Figure 1. The RASEX measurement site. The three towers in RASEX are designated as SMW (sea mast west), SMS (sea mast south), and LM (land mast). All observations in this study were collected at the SMW location.

All quality control and flux sampling procedures in Vickers and Mahrt (1997) were applied to the 10 m sonic anemometer data. Seven 1 hour data records were identified as having instrument problems and were discarded. Ninety-nine records were discarded for having large relative systematic flux errors (>0.75), large relative random flux sampling errors (>0.75), and large flux-event index (>3) in either the virtual heat flux or the wind stress vector (see Vickers and Mahrt, 1997). The flux sampling criteria identify predominantly light wind speed cases, where the flux can be strongly nonstationary. A total of 106 data records out of 546 were discarded by the quality control and flux sampling criteria applied to the 10 m sonic data, leaving 440 one hour records within a one month period.

The fluctuating wave height was measured using an acoustic wave recorder logged at a frequency of 20 Hz and thought to be reliable at frequencies of approximately 10 Hz and lower. Wave heights from the fast response (20 Hz) wave wire number three instrument are also analyzed. The currents were measured with an electromagnetic current registration system developed by Geological and Marine Instrumentation.

2.1. FLUXES AND DRAG COEFFICIENT

Turbulent fluctuations of some quantity, ϕ, are defined as deviations from a local average, $\bar{\phi}$, in which case the decomposition of ϕ can be written as

$$\phi = \bar{\phi} + \phi', \tag{2}$$

where $\bar{\phi}$ is an average over the local time scale. The local time scale defines the longest time scales of the motions included in the turbulent flux. In order to provide a stable estimate of the flux with small random flux sampling error, it is necessary to average the flux over a period which may be longer than the local time scale used in Equation (2). We choose a local time scale of 10 minutes based on the scale dependence of the wind stress magnitude, and choose the flux averaging period to be one hour based on the scale dependence of the correlation between the mean flow and the wind stress (Mahrt et al., 1996). The magnitude of the kinematic turbulent wind stress is calculated as

$$\tau/\rho = (\langle w'u' \rangle^2 + \langle w'v' \rangle^2)^{1/2} = u_*^2, \tag{3}$$

and the relative wind speed as

$$U = (\langle u - u_c \rangle^2 + \langle v - v_c \rangle^2)^{1/2}, \tag{4}$$

where the $\langle\ \rangle$ operator represents an average over the one hour record, u_c and v_c are the components of the current in the direction of the wind components and u_* is the friction velocity.

The 10 m drag coefficient, C_d, was reduced to neutral stability to facilitate comparisons with other studies. The neutral drag coefficient, C_{dn}, was calculated using the implicit expression of Geernaert and Katsaros (1986),

$$C_{dn} = \left[C_d^{-1/2} + \frac{\Psi}{\kappa} - \frac{1}{\kappa} \ln \left(\frac{C_{dn}}{C_d} \right) \right]^{-2}, \tag{5}$$

where κ is von Karman's constant (=0.4) and Ψ the atmospheric stability function for momentum (Paulson, 1970). The third term on the right hand side of Equation (5) is derived based on the Charnock (1955) prediction that the roughness length is proportional to u_*^2/g. For wind speeds less than 4 m s^{-1}, such an assumption may not be valid, and we use the simpler terrestrial form where the roughness length is assumed constant and the third term on the right hand side of Equation (5) is set to zero. Stability effects are most important for weak wind cases. Unfortunately, reducing the drag coefficients to their neutral values still leaves substantial dependence on stability. It is not known if the failure of similarity theory is due to a) inadequacy of the form of the stability functions (Ψ), b) general failure of the Charnock relationship or assumption of constant roughness length in the reduction to neutral stability, c) failure of Monin-Obukhov similarity theory due to the

importance of additional length scales, or d) large errors in the fluxes and Obukhov length (L) at weak wind speeds which are not eliminated by the quality control process (Mahrt et al., 1996). As a result of these difficulties, data characterized by $|z/L| > 0.5$ will be retained in our general analyses (Section 3) but excluded from the modelling formulations in Sections 4 and 5 to reduce the influence of stability. In this study, values of the drag coefficient will be reported in units of 10^{-3}.

At weak wind speeds, choices between use of the vector and scalar averaged wind speed and choice between the total stress and the stress in the mean wind direction all can affect the calculated drag coefficient values (Mahrt et al., 1996). Perrie and Toulany (1990) found the need to use only the stress component in the direction of the waves at the peak frequency while some other studies have included only the stress component aligned with the wind. Here we include the total stress and vector-average both the wind stress (Equation (3)) and the wind speed (Equation (4)).

2.2. WAVE STATE

The wave state is described from spectra of the observed fluctuating wave height (Højstrup, 1994). The temporal resolution of the acoustic wave recorder precludes measurement of the high-frequency gravity-capillary waves but is sufficient to capture the dominant gravity wave mode. The wave height spectra for RASEX typically show a narrow peak centered on a period between 1.5 and 3.5 seconds.

Three spectral methods were applied to the acoustic wave data to obtain estimates of the characteristic wave period (Højstrup, 1994). With the first method, the characteristic frequency is defined where 50% of the accumulated variance is obtained. The second method is based on the mean frequency and is calculated as the ratio of the first and second spectral moments. The third method is based on the zero crossing frequency and is the square root of the ratio of the first and third spectral moments. All three of these measures of characteristic frequency are highly correlated with each other ($R > 0.94$). For this analysis, we select the characteristic frequency based on the 50% accumulated variance method.

The characteristic wave number is calculated using the dispersion relationship for finite water depth and ignoring surface tension so that

$$\omega^2 = gk \tanh(kD), \tag{6}$$

where ω is the characteristic radian frequency, g the acceleration of gravity, k the characteristic wave number and $D = 4$ m the water depth. The dispersion relation is solved for wave number, which provides the wave phase speed, $C_p = \omega/k$, of the dominant gravity wave. We calculate wave age parameters as the ratio of the wave phase speed to either the friction velocity (Equation (3)) or the 10 m wind speed (Equation (4)).

An estimate of the width of the wave height spectra is calculated as the frequency bandwidth which includes the 25% to the 75% percentiles of the accumulated

variance distribution. The bandwidth is a measure of the complexity of the wave field. Wave spectra with multiple wave number modes of similar amplitude correspond to large values of the bandwidth. In the open-ocean case, large bandwidth can occur when the wave height is a mixture of locally wind-generated waves and swell (e.g., Rieder, 1997), where open-ocean swell is typically characterized by wave modes with periods in excess of 10 seconds. For the RASEX inland sea location, which is always fetch limited compared to the open-ocean case, the wave height spectra rarely show clear separation between higher frequency wind-driven waves and lower frequency swell.

As a check on the acoustic wave data, the characteristic frequency and the frequency bandwidth were calculated using the independent wave wire data set and the accumulated variance method. The dominant wave periods from the acoustic recorder and from the wave wire are correlated with $R = 0.99$. The mean wave period from the acoustic recorder is larger than that from the wave wire by 0.06 s. The frequency bandwidth comparison shows that the acoustic recorder and the wave wire agree with a correlation of $R = 0.96$. The mean estimate of the bandwidth from the wave wire is only 0.02 s^{-1} wider than that from the acoustic recorder. In the remainder of this study, we use the acoustic wave recorder data and the accumulated variance method to calculate the characteristic frequency and the frequency bandwidth.

We estimate the significant wave amplitude, A, from the standard deviation of the total wave height σ_{wave}

$$A = 4\sigma_{\text{wave}}. \tag{7}$$

The wave amplitude defined in this way is equivalent to the crest-to-trough height exceeded by one-third of the waves.

3. Results

Figure 2 shows the mean, standard error and standard deviation of the 10 m drag coefficient reduced to neutral stability, C_{dn}, as a function of the relative 10 m wind speed, U, for off and on-shore flow conditions (also see Figure 3j). The mean, standard error and sample size of the neutral drag coefficient for wind speed categories are tabulated in Table I. The solid curve in Figures 2a and 2b is the sum of the Charnock (1955) prediction for the drag coefficient for a mature wave state, $z_{oc} = 0.011\, u_*^2/g$, plus the smooth flow contribution, $z_{os} = 0.11\, \nu/u_*$ (e.g., Fairall et al., 1996), referred to in this section as the modified Charnock relationship. For off-shore flow, the RASEX drag coefficient is larger than the modified Charnock relationship, while in on-shore flow with moderate wind speeds, the RASEX drag coefficient is slightly smaller than the modified Charnock relationship. Compared to the open-ocean situation, the RASEX data are characterized by fetch limited conditions for both off and on-shore flow, a near absence of large amplitude swell, and

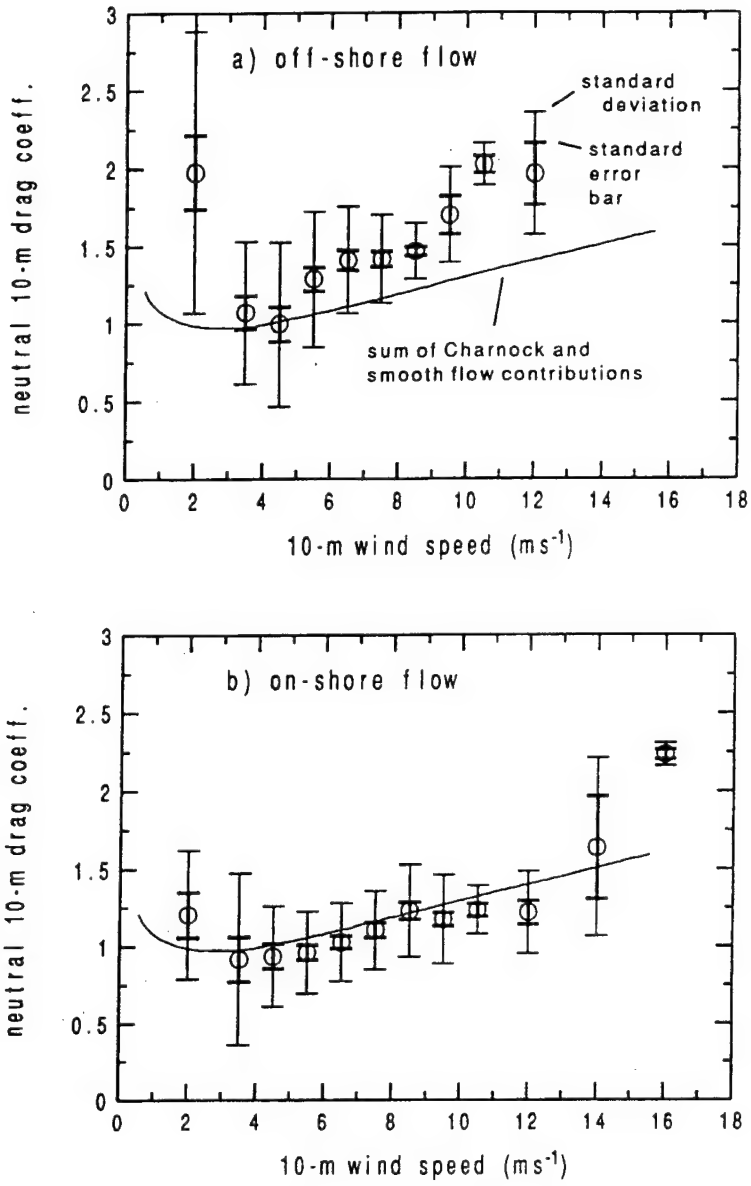

Figure 2. Mean values (circles), plus or minus one standard error (thick bars) and plus or minus one standard deviation (thin bars) of the neutral 10 m drag coefficient as a function of the relative 10 m wind speed (m s^{-1}) for (a) off-shore and (b) on-shore flow. The solid curve in both panels is the sum of the Charnock and the smooth flow contributions to the roughness length using a Charnock constant of 0.011.

the potential for shallow water waves. The variability of the neutral drag coefficient (standard deviation in Figure 2) not explained by wind speed is substantial.

Comparison of on and off-shore flow (Figure 3j) shows that, a) the off-shore drag coefficient is larger for all wind speed categories, b) the drag coefficient for off-shore flow increases more rapidly with increasing wind speed for wind speed greater than 4 m s^{-1}, c) the drag coefficient is a minimum for wind speeds of about 4 m s^{-1} for both on- and off-shore flow, and d) the drag coefficient for on-shore

Table I
Neutral 10 m drag coefficient in units of 10^{-3}

	Off-shore flow			On-shore flow		
U m s^{-1}	Mean	Stderr	N	Mean	Stderr	N
1–3	1.98	0.23	15	1.20	0.15	8
3–4	1.07	0.11	18	0.92	0.14	15
4–5	0.99	0.11	23	0.93	0.08	16
5–6	1.28	0.08	33	0.96	0.05	30
6–7	1.41	0.07	28	1.03	0.04	40
7–8	1.42	0.05	31	1.10	0.05	28
8–9	1.47	0.03	37	1.23	0.06	27
9–10	1.70	0.13	6	1.17	0.05	41
10–11	2.02	0.06	6	1.24	0.04	14
11–13	1.96	0.20	4	1.22	0.08	12
13–15	–	–	0	1.63	0.33	3
15–17	–	–	0	2.23	0.03	5

flow increases rapidly with wind speed for wind speeds greater than 12 m s^{-1}, apparently due to wave breaking.

The increase of the drag coefficient with wind speed for wind speeds greater than 4 m s^{-1}, may be related to the increase of wave amplitude and wave slope with increasing wind speed (Figures 3c and 3d). The larger drag coefficient for off-shore flow waves is consistent with the concept of younger growing waves which efficiently extract momentum from the wind field. The frequency bandwidth of the wave spectra is larger for off-shore flow than on-shore (Figure 3f), suggesting that in addition to wave age, the presence of multiple wave modes during off-shore flow may also act to enhance the drag coefficient.

The drag coefficient is larger for the lightest wind speed category (1 to 3 m s^{-1}) than for wind speeds near 4 m s^{-1}, especially for off-shore flow (Figures 2 and 3j). Some of this increase in the drag coefficient at light winds may be due to flux sampling problems due to the greater importance of nonstationarity, and the increased influence of stability compared to stronger wind cases (Mahrt et al., 1996). The largest flux sampling errors remaining after the flux error criteria are applied (Section 2) occur at the lightest wind speeds. In Figures 2 and 3, we have not discarded any data because of large stability effects, and any errors made in reducing the drag coefficient to neutral stability will introduce error in the neutral drag coefficient. Despite these problems, the increased drag coefficient in light wind speeds appears to be real.

The drag coefficient at light wind speeds in off-shore flow is twice as large as that predicted by the sum of the mature wave state Charnock plus smooth flow contributions to the roughness length (Figure 2a). The enhancement of the drag coefficient at light winds may be due to broad wave spectra associated with multiple

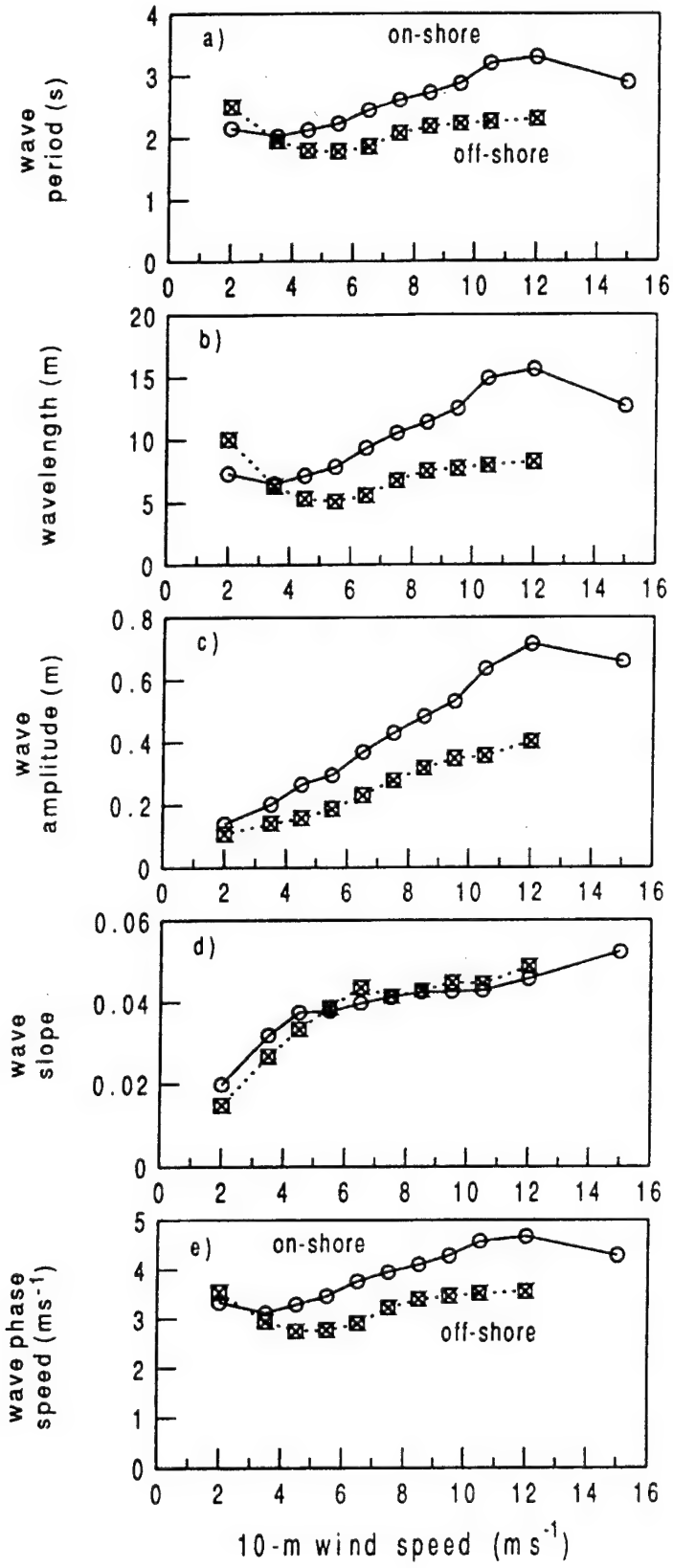

Figure 3. Mean values of the (a) characteristic wave period (s), (b) wave length (m), (c) wave amplitude (m), (d) wave slope, (e) wave phase speed (m s^{-1}), (f) frequency bandwidth (s^{-1}), (g) (C_p/u_*) wave age, (h) (C_p/U) wave age, (i) high-pass filtered wave height variance (m^2), and (j) neutral 10 m drag coefficient, as a function of the relative 10 m wind speed (m s^{-1}) for off-shore (squares and dotted lines) and on-shore (circles and solid lines) flow.

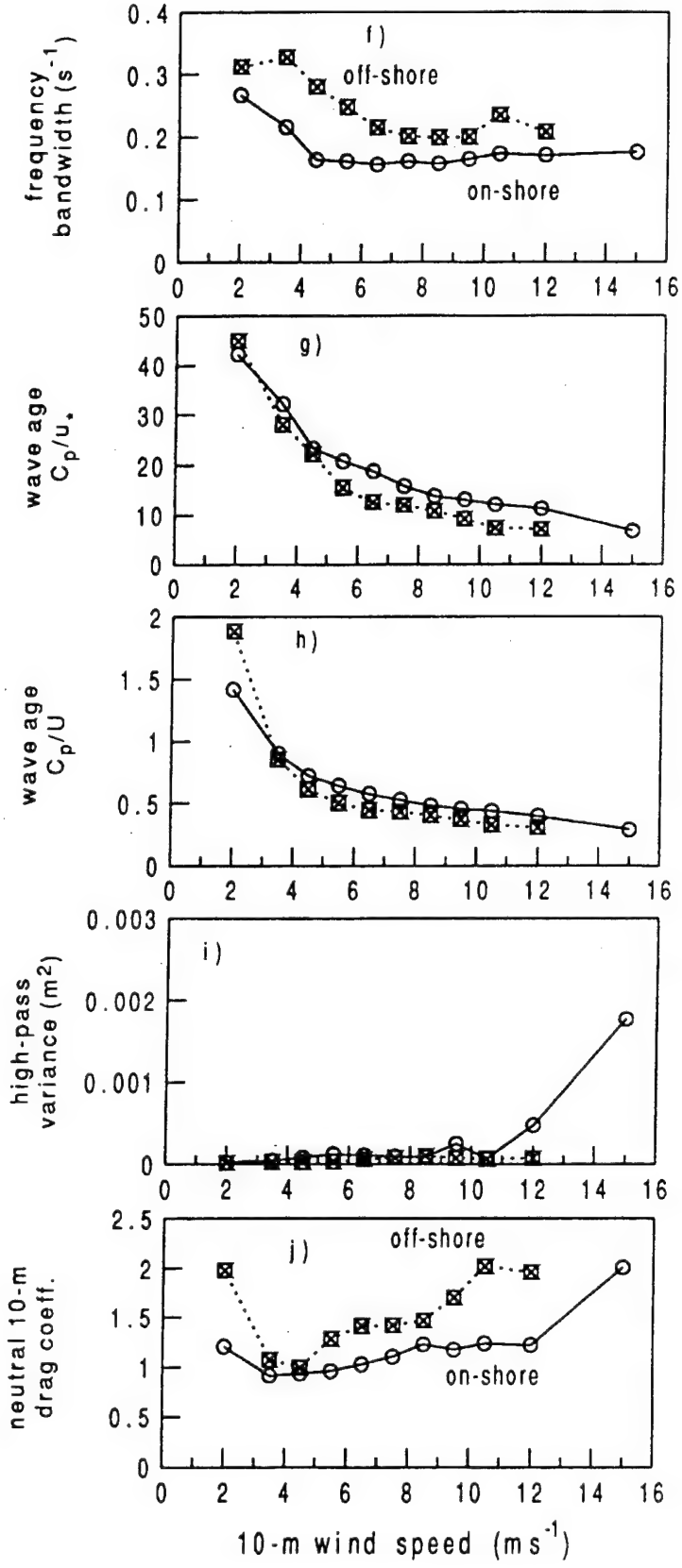

Figure 3 (continued).

wave modes, some of which are probably not aligned with the wind. In light winds, the wind direction is generally more variable and the wave field is less able to maintain equilibrium with the wind field. Also in light winds, the dominant wind-wave mode has smaller amplitude and wave modes not directly coupled to the local wind may become relatively more important even when small.

Despite the fact that these observations are in shallow water, the wave phase speed (Figure 3e) is within 5% of the deep water prediction ($(gk)^{0.5}/k$), 95% of the time, primarily because the wave length and wave amplitude in RASEX are small (Figures 3b and 3c). Modification of the wave phase speed due to finite water depth becomes important when the wave length exceeds four times the water depth, or equivalently for RASEX, when the wave period exceeds 3.4 seconds. There are only 20 data records where the wave period exceeds this value and most of these cases occur with strong steady on-shore flow and apparent wave breaking.

While no visual observations of wave breaking are available, wave breaking is suggested by the following observations for on-shore flow with winds exceeding 12 m s^{-1}. For these conditions (Figure 3): a) the wave amplitude no longer increases with wind speed, b) the wave slope and drag coefficient increase significantly with wind speed and reach the largest observed values for these data, c) the dominant wave phase speed reaches a maximum and then decreases with wind speed, or equivalently, from the dispersion relationship, the dominant gravity wave length approaches four times the water depth where it is a maximum, and d) the 1 second high-pass filtered wave height variance from the wave wire becomes very large (Figure 3i). These results suggest that for on-shore flow greater than 12 m s^{-1} wave breaking occurs which is expected to enhance the drag coefficient (Banner and Melville, 1976; Banner, 1990). With strong on-shore winds, the waves may be long enough to interact with the bottom leading to wave steepening and wave breaking (shoaling) which limits the wave amplitude and wave length and reduces the wave phase speed.

For all wind speeds, the drag coefficient decreases with increasing wave age (move vertically in Figure 4). For all but the smallest values of the wave age parameter ($C_p/u_* < 8$), the drag coefficient decreases with wind speed for a fixed wave age category. That is, the friction velocity is relatively constant for a given wave age category which generally requires the drag coefficient to decrease with wind speed for a given wave age category.

The drag coefficient for the category of smallest wave age parameter (C_p/u_* between 4 and 8) increases with wind speed (Figure 4). This small wave age category occurs with strong on-shore flow. We attribute the different characteristics of the small wave age class to wave breaking which increases with wind speed. This causes the drag coefficient to increase with wind speed. Notice that for the wave breaking case, the small values of the wave age parameter are not due to the actual 'young age' of wind-driven waves but rather to the reduction of the phase speed by wave breaking. In this sense, the wave age parameter represents two distinctly different effects, the influence of the age of wind-driven waves and the influence of

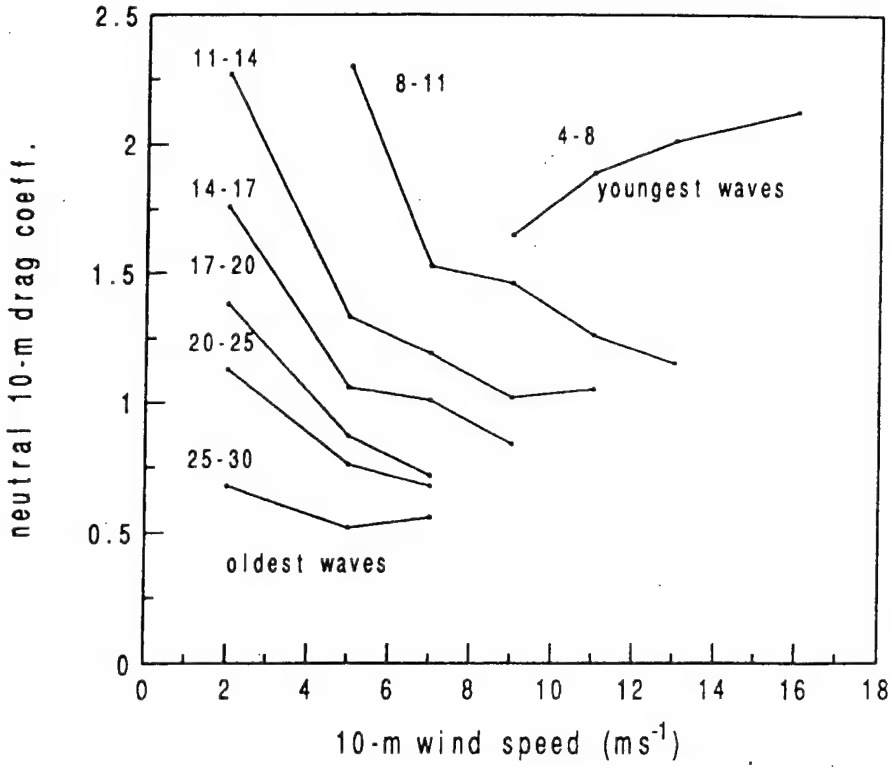

Figure 4. Mean values of the neutral 10 m drag coefficient as a function of the relative 10 m wind speed (m s^{-1}) for 7 wave age (C_p/u_*) categories.

wave breaking and possibly bathymetry through shoaling. We note that the detailed nature of the reduction in wave phase speed and wave age due to wave breaking may be site specific.

For the present data, the drag coefficient increases with decreasing wave age down to the smallest observed wave age values near 5. Previous studies have suggested that for moderate coastal fetch, the drag coefficient is a maximum for a wave age of 10 (Nordeng, 1991) and 7 (Geernaert and Smith, 1997) and smaller for smaller values of the wave age. However, we associate the smallest wave age in RASEX with wave breaking, which probably enhances the drag coefficient.

3.1. Comparison with other studies

The RASEX off-shore flow drag coefficients agree reasonably well with those reported by Donelan (1982) from data collected near the coast of Lake Ontario, Canada (compare line 3 with line 10 in Figure 5). The off-shore flow drag coefficients for RASEX are also similar to those reported in Smith et al. (1992, Figure 11) for young growing waves (values of the wave age parameter $C_p/U = 0.5$). For wind speeds greater than 12 m s^{-1} in on-shore flow, the RASEX drag coefficients increase with increasing wind speed at a rate which exceeds any of those summa-

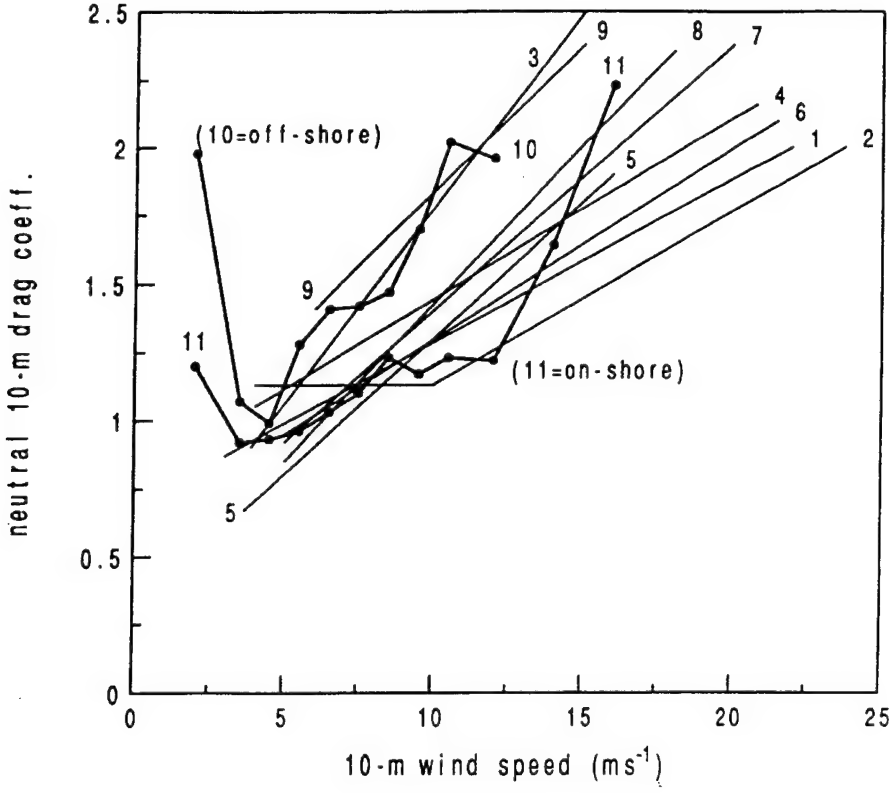

Figure 5. Published drag coefficient-wind speed (m s^{-1}) regression equations: 1) Smith (1980), 2) Large and Pond (1981), 3) Donelan (1982), 4) Garratt (1977), 5) Sheppard et al. (1972), 6) Smith and Banke (1975), 7) Geernaert et al. (1986), 8) Smith et al. (1992), 9) Smith et al. (1992) 'very young waves', 10) off-shore flow in this study, and 11) on-shore flow in this study.

rized in Figure 5 by nearly a factor two. We attribute this to wave breaking possibly associated with shoaling.

Our analysis of the thrust anemometer data reported by Smith (1980, Tables 1 and 2) also shows larger neutral drag coefficients in off-shore flow compared to on-shore flow, for a given wind speed, presumably due to younger growing waves in off-shore flow. These data were collected on an anchored spar buoy in 59 m of water 10 km off the coast of Nova Scotia, Canada. In our analysis of these data, we considered off-shore flow to include fetches between 10 km and 20 km and on-shore flow to be unlimited fetch. The 10 m drag coefficients in Smith (1980, Tables 1 and 2) were reduced to neutral using Equation (5), and runs with values of the stability parameter (z/L) greater than 0.5 in magnitude were discarded. For off-shore flow and the same wind speed, the 10 m neutral drag coefficient in RASEX is approximately 35% larger than that reported by Smith, probably due to the shorter fetch at the RASEX site.

In the open-ocean and deep water data of Rieder (1997), the wave age parameter (C_p/u_*) is larger than observed in RASEX. His wave age ranges from 19 to 172. His large values of wave age may be due to very old seas containing fast moving

large amplitude swell not related to the local wind. The wave phase speeds range from 6 to 23 m s^{-1} compared to 1.8 to 5.2 m s^{-1} for RASEX. For a given value of wave age, the open-ocean drag coefficients calculated by Rieder are much larger than those found for RASEX. The drag coefficients in Rieder have no correlation with wind speed ($R^2 < 0.01$), and weak correlation with wave age ($R^2 = 0.15$). Rieder concludes that in general, the complexity of swell dominated seas is not included in historical formulations of the drag coefficient based on wind speed and wave age. In complex swell, the differences between the direction of the swell, wind-driven waves, wind stress and the wind vector can result in large scatter in the drag coefficient, not explained by either wind speed or wave age. For example, in the data of Rieder (1997), the wind sometimes blew opposite to the wave propagation direction, at least for some wave frequency bands.

Both the data of Rieder (1997) and the model of Geernaert et al. (1987) suggest significantly larger drag coefficients *for a given wave age* than those observed in RASEX. The drag coefficients in coastal situations (Garratt, 1977; Wu, 1980; Geernaert et al., 1987) are on average larger than the drag coefficients in the open-ocean (Smith, 1980; Large and Pond, 1981) because of fetch-limited developing seas. However, for a given wave age, the drag coefficients are larger over the open ocean, apparently due to the presence of multiple wave modes.

3.2. TIME DEPENDENT EXAMPLE

The RASEX data show that the drag coefficient depends both on wind speed and wave age, which suggests that the drag coefficient cannot be adequately formulated in terms of wind speed and stability alone. In this section, we analyze a three day period of on-shore flow with moderate wind speeds where stability effects are not important (Figure 6). The upwind fetch distance is nearly constant during this period although the wind direction is not. For this three day period, the drag coefficient is highly related to inverse wave age ($R^2 = 0.89$) and less correlated with wind speed ($R^2 = 0.20$), although part of the large correlation with inverse wave age is due to built-in correlation (Section 4).

During period 1 (day 284.0–284.5), the drag coefficient increases by a factor of two as the wind accelerates and the wave age decreases. However, for much of the three day period, variations of the drag coefficient are unrelated to wind speed. For example, during period 2 (day 285.0–285.5), the wind speed is almost constant while the drag coefficient steadily decreases and the wave age increases. The increase of wave phase speed and wave age and the decrease of the stress with time (Figure 6) are consistent with a maturing wave field. In period 3 (day 286.5–287.0), the wind vector is relatively constant but the stress and the drag coefficient increase by nearly a factor of 2. The increasing drag coefficient occurs with decreasing phase speed and wave age.

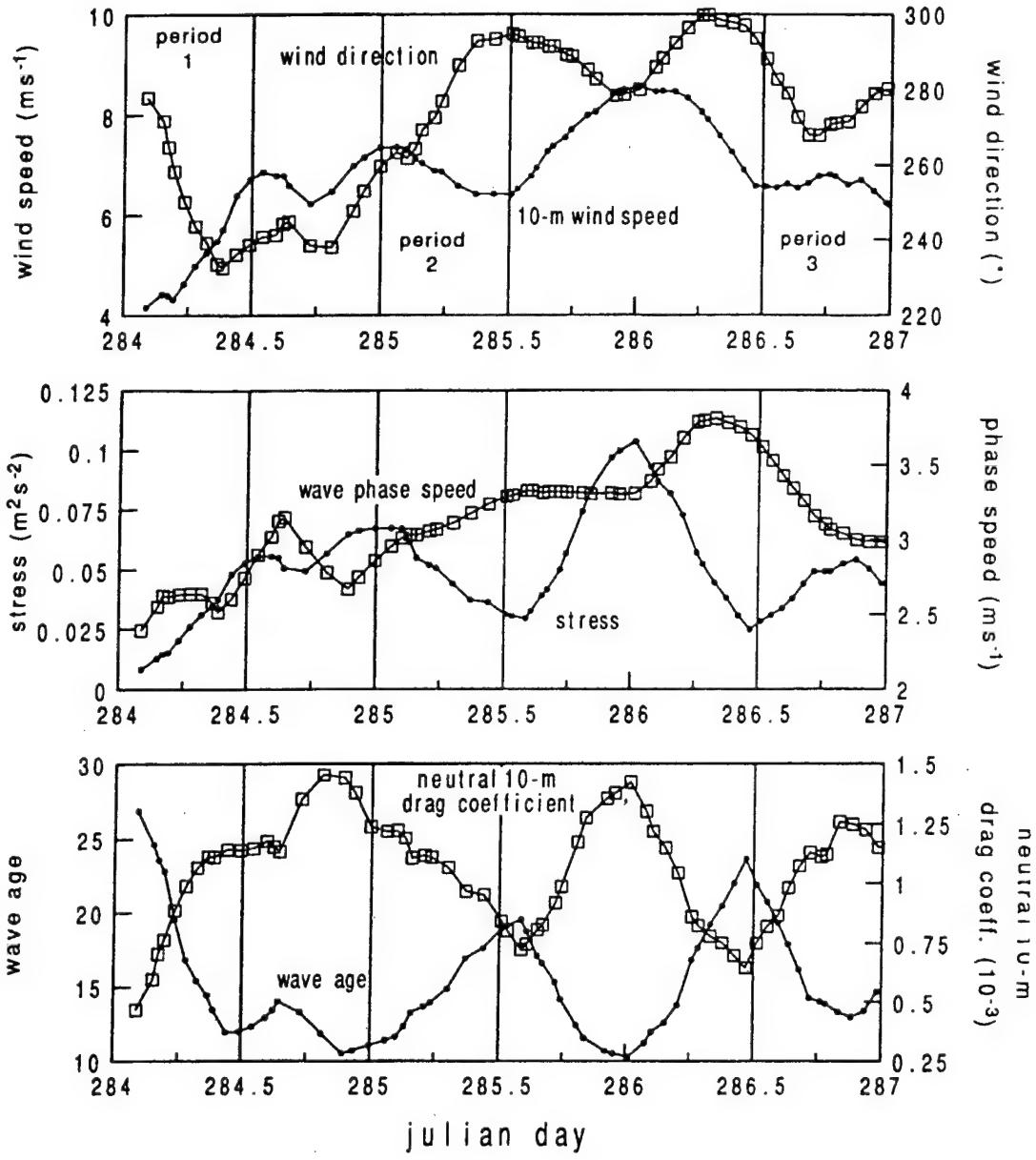

Figure 6. Time series of six hour running mean quantities for days 284 through 287 of (a) the relative 10 m wind speed (m s^{-1}) and 20 m wind direction, (b) wind stress (m^2 s^{-2}) and wave phase speed (m s^{-1}), and (c) wave age (C_p/u_*) and the neutral 10 m drag coefficient.

3.3. FLOW ACCELERATION

Since the drag coefficient for a given wind speed is larger with young developing waves, the drag coefficient is expected to be larger with flow acceleration, as observed by Large and Pond (1981) and Smith (1980). In fact, the stress may become very small or even reverse sign with significant deceleration implying small or negative drag coefficients (Smedman et al., 1994). We quantify the non-stationarity of the flow by linearly regressing the along-wind component on time

to estimate the difference in the along-wind component between the beginning and end of the one hour record, δu. This difference is normalized by the mean along-wind component, $[u]$, to give the relative nonstationarity

$$RNu = \delta u/[u]. \tag{8}$$

Positive (negative) RNu corresponds to accelerating (decelerating) winds over the record.

Comparison of the neutral drag coefficient as a function of wind speed for $RNu > 0$ and $RNu < 0$ classes for off and on-shore flow shows no significant difference between the accelerating and decelerating classes. This is probably due to the fact that, for these data, flow acceleration only occasionally determines the wave state. The next subsection includes an example where a change of wind direction leads to multiple wave modes and an enhanced drag coefficient.

3.4. FREQUENCY BANDWIDTH

The frequency bandwidth in RASEX is largest for weak wind speed and tends to be larger in off-shore flow (Figure 7). With strong on-shore winds, the wind-driven wave mode is dominant, lower frequency swell is unimportant and the wave height spectra are characterized by a single large amplitude narrow peak. In strong off-shore flow, the wave height spectra have smaller peak amplitude and larger bandwidth compared to strong on-shore flow. Since the wind-driven waves have smaller amplitude in off-shore flow, wave motions at frequencies other than the characteristic frequency become relatively more important compared to the on-shore case. The bandwidth is largest in light winds for both on and off-shore flow due to multiple wave modes (Figure 7).

An example of the change in frequency bandwidth corresponding to a change in wind direction from on-shore to off-shore flow is shown in Figure 8. The relatively narrow spectra of the dominant wind-driven wave mode in moderate on-shore flow broadens toward lower frequencies when the wind shifts to off-shore. The lower frequency wave modes in the broad spectra could be interpreted as slowly decaying waves from the on-shore flow wind regime of four hours previous. The bandwidth is large in this case because the wave heights are a mixture of the old decaying waves and the new growing waves. For this example, the neutral drag coefficient is enhanced when the wind shifts to off-shore flow and the bandwidth broadens.

4. Drag coefficient models

This section tests existing formulations of the drag coefficient and constructs a new model which better describes the RASEX data. The following is not physically rigorous, but rather attempts to examine how well simple models can approximate

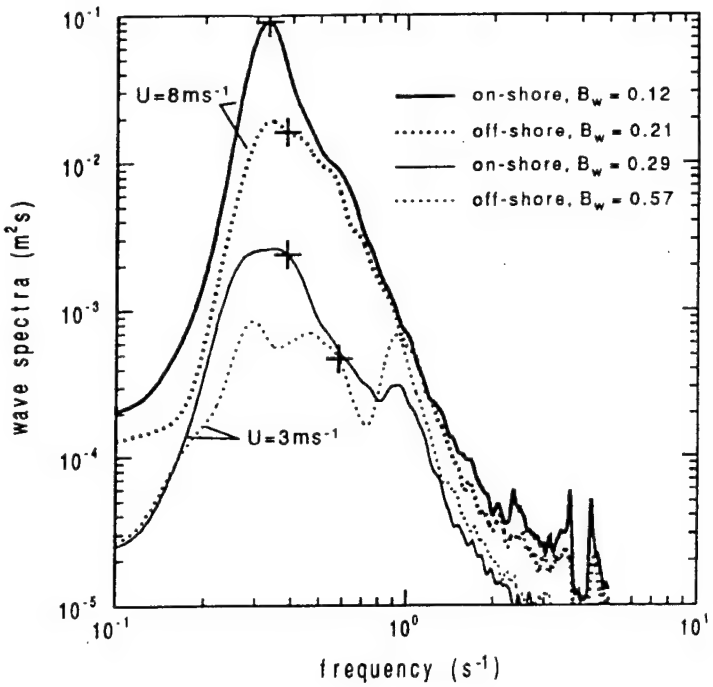

Figure 7. Typical wave height spectra for weak and strong on-shore flow (solid lines) and weak and strong off-shore flow (dotted lines). The frequency bandwidth (B_w) has units of s^{-1}. The characteristic frequency for each spectra is denoted by a plus sign.

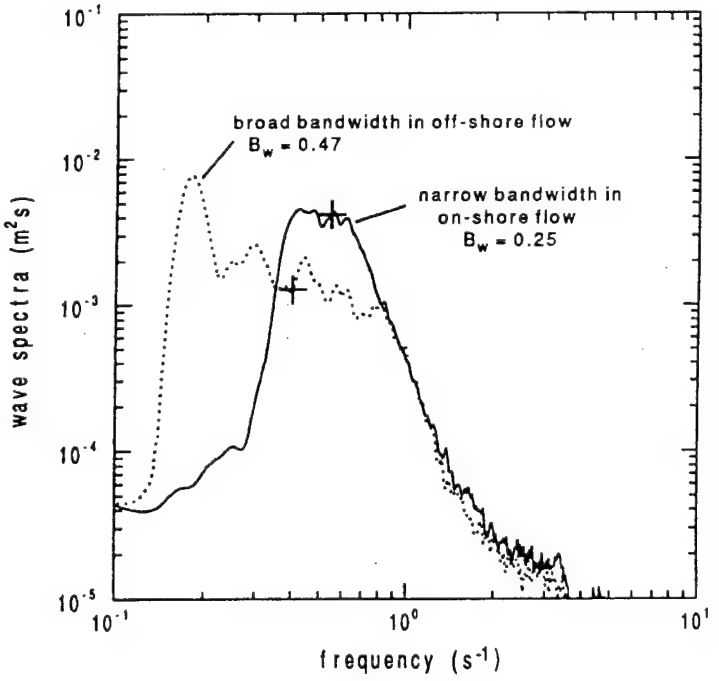

Figure 8. Time change of wave height spectra for a wind shift from 5 m s^{-1} on-shore flow (solid line) to 4 m s^{-1} off-shore flow (dashed line) 4 hours later. The frequency bandwidth (B_w) has units of s^{-1}. The characteristic frequency for each spectra is denoted by a plus sign.

the wind stress in the complex coastal zone without explicitly including wind-wave-stress directional differences, multiple wave modes and potential effects of shoaling and bottom topography. The modelling strategy will be to formulate the neutral 10 m drag coefficient in terms of bulk wave state parameters and wind speed. The modelled stability dependent drag coefficient (C_d) can be calculated from the neutral value (C_{dn}) and the atmospheric stability function for momentum Ψ using the expression of Geernaert and Katsaros (1986) (Equation (5)).

4.1. DIRECT MODELS

The neutral drag coefficient increases with wind speed for $U > 4$ m s^{-1} with large scatter and increases with inverse wave age with less scatter (Figures 9a and 9b), although part of the variance explained by inverse wave age is due to self-correlation (discussed below). In both cases, the scatter is largest when stability effects are important.

Cases with $|z/L| > 0.5$ (see Figures 9a and 9b) are excluded from all subsequent analyses to reduce effects of non-neutral stability which in RASEX could not be adequately removed by the usual reduction to the neutral drag coefficient. Our motivation for removing these cases is to study the effects of wind speed and wave state on the drag coefficient. This exclusion eliminates most cases of strong upward buoyancy flux associated with cold air advection and internal boundary layers. Thirty-eight out of 440 data records are discarded because of strong stability effects, leaving 402 one hour records. For the remaining cases, the stability adjustment (Equation (5)) is applied but is generally less important.

The historical regression formulation for the drag coefficient in terms of wind speed for wind speeds larger than 4 m s^{-1} explains only 14% of the variance of the neutral drag coefficient for RASEX,

$$C_{dn} = 0.75 + 0.067U;\ U > 4\ \text{m s}^{-1};\ R^2 = 0.14. \tag{9}$$

The wind speed model does poorly because it does not include any information on wave state. Modelling the drag coefficient in terms of wind speed would be improved by partitioning the data into on and off-shore flow and developing a separate model for the two cases.

An inverse wave age parameter based on wind speed (U/C_p), for wind speeds larger than 4 m s^{-1}, predicts more than twice as much variance in the drag coefficient in RASEX compared to the model based on wind speed alone,

$$C_{dn} = 0.26 + 0.46(U/C_p);\ U > 4\ \text{m s}^{-1};\ R^2 = 0.34. \tag{10}$$

This result shows that the phase speed of the dominant gravity wave (C_p) explains significant variance of the drag coefficient not explained by wind speed.

When analyzing all wind speeds, the wave age parameter in terms of friction velocity (C_p/u_*) explains significantly more variance of the drag coefficient compared to wave age in terms of wind speed (C_p/U), even after removing variance

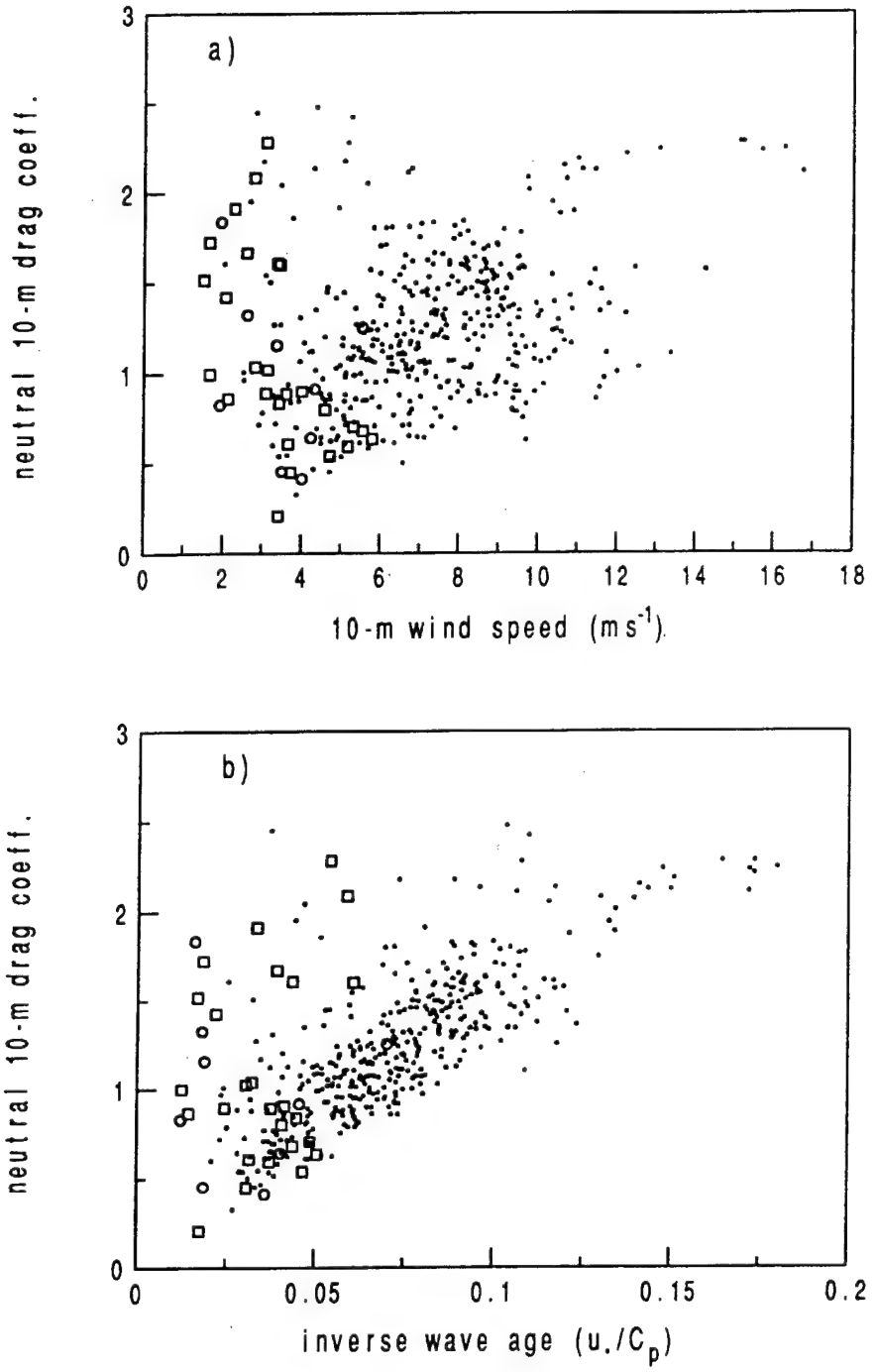

Figure 9. The neutral 10 m drag coefficient as a function of (a) the relative 10 m wind speed (m s^{-1}) and (b) inverse wave age (u_*/C_p). Data points with $z/L < -0.5$ (unstable) are shown as squares and $z/L > 0.5$ (stable) are shown as circles.

explained due to self-correlation. The model based on C_p/u_* describes the entire wind speed range whereas the models based on wind speed or U/C_p would require separate models for weak and strong wind conditions. Wave age raised to the

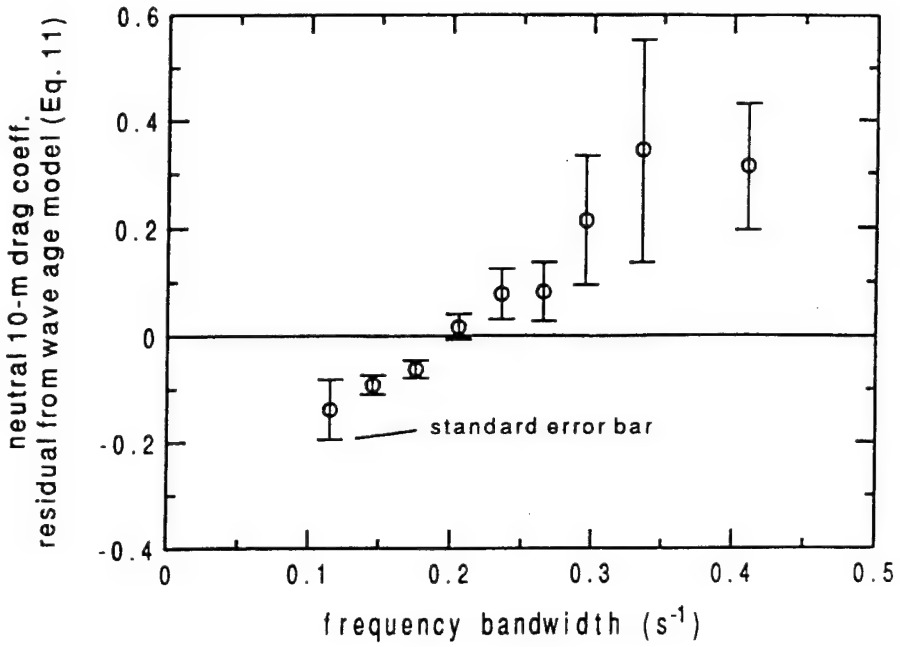

Figure 10. The neutral 10 m drag coefficient residuals from the wave age model (Equation (11)) as a function of the frequency bandwidth (s^{-1}) of the wave height spectra.

minus two thirds power (Geernaert et al., 1987) explains the same variance of the drag coefficient as a linear inverse wave age model and has the advantage that the constant term is essentially zero. The regression model for the RASEX data yields

$$C_{dn} = 7.1(C_p/u_*)^{-2/3}; \;\; R^2 = 0.58. \tag{11}$$

The range of wave age (C_p/u_*) observed for RASEX is 5.6 to 48, and application of the above model to wave ages outside this range can not be tested.

A drag coefficient model in terms of wave age based on the friction velocity (Equation (11)) includes built-in self-correlation since the drag coefficient is also proportional to u_* (see, for example, Smith et al., 1992). A numerical experiment in which the observed (U, u_*, C_p) triplets were individually randomly re-distributed with one-thousand realizations shows that the average built in self-correlation with inverse wave age can explain 27% of the variance of the drag coefficient. The variance of the drag coefficient explained by the inverse wave age model (Equation (11)) is more than twice as large as that expected from self-correlation.

The residuals from the drag coefficient model (Equation (11)) are positively correlated with the frequency bandwidth of the wave spectra (R = 0.43) (Figure 10). When the bandwidth is small, the wave field is characterized by a single dominant gravity wave mode and the wind stress is less, for a given wave age and wind speed. With large bandwidth, the wind stress is large for a given wave age and wind speed due to enhanced drag from multiple wave modes.

The RASEX observations suggest that much of the variability of the neutral drag coefficient not explained by the wave age parameter is proportional to the

frequency bandwidth (B_w) of the waves and inversely proportional to wind speed. An excellent fit to the RASEX data can be obtained by modelling the neutral drag coefficient as

$$C_{dn} = -0.5 + 8.9(C_p/u_*)^{-2/3} + 0.9(B_w\lambda/U); \;\; R^2 = 0.71, \tag{12}$$

where λ is the wave length of the dominant wave and is included here on dimensional grounds. This relationship is valid only within the ranges of wave age and the dimensionless broad spectrum parameter ($B_w\lambda/U$) of the data and is not valid in the limit of vanishing wave age, bandwidth or wind speed. The observed range of the dimensionless broad spectrum parameter in RASEX is 0.07 to 2.4. The addition of the frequency bandwidth term is statistically significant at the 99% level and much of the unexplained variance is probably due to flux sampling problems primarily in light winds. The regression coefficients and variance explained by the model (Equation (12)) are nearly identical when partitioning the data into off and on-shore cases.

Equation (12) predicts that for a given wave age and wind speed, the drag coefficient will be larger with large bandwidth. For RASEX, the largest values of bandwidth occur during light winds when the amplitude of the dominant wind-driven gravity wave mode is relatively small. For moderate and strong wind speeds, the bandwidth is not related to wind speed (Figure 3f). In the open-ocean case, the bandwidth parameter may describe the enhancement of the drag coefficient due to swell, and may explain the larger drag coefficients in the open-ocean compared to on-shore flow in RASEX for a given wave age.

4.2. ROUGHNESS LENGTH FORMULATIONS

In this section, values of the drag coefficient are computed based on existing models of the roughness length. We will test whether or not these formulations can approximate the drag coefficient in the coastal zone where wind-wave-bottom interactions may be complex and very young seas are common.

A roughness length model that scales the Charnock prediction of the roughness length by an inverse wave age dependence (Toba and Koga, 1986; Maat et al., 1991; Donelan, 1990; Smith et al., 1992), and adds the smooth flow contribution (Fairall et al., 1996), is

$$z_o = (u_*^2/g)K(u_*/C_p)^p + 0.11\nu/u_*, \tag{13}$$

where ν is the viscosity of air and K and p are empirical parameters. Alam and Curry (1997) include an additional term due to parameterized surface tension and attach additional conditions to model the smooth flow case where the first term on the right side of Equation (13) is set to zero. Both the smooth flow contribution and the parameterized surface tension term were found to be small for most of the RASEX data where extended calm conditions were rare. The first term on the right

hand side of Equation (13) includes the original formulation of Charnock (1955) for fully developed sea states (large wave age),

$$z_{oc} = \alpha(u_*^2/g) \tag{14}$$

where α is the Charnock 'constant' or dimensionless roughness length. The neutral drag coefficient is related to the roughness length as

$$C_{dn} = \left(\frac{\kappa}{\ln(z/z_o)}\right)^2. \tag{15}$$

The coefficients $K = 0.48$ and $p = 1$ (Equation (13)) were empirically determined from data collected at an off-shore platform in the North Sea, 9 km from the coast in 18 m of water during the Humidity Exchange over the Sea (HEXOS) experiment (Smith et al., 1992).

The Charnock formulation (Equation (14)) explains 43% of the variance of the neutral drag coefficient for RASEX. However, applying the same self-correlation test from Section 4.1 to the Charnock model (Equation (14)) shows that the average built-in correlation explains 35% of the total variance of the drag coefficient. Thus, the Charnock model predicts very little of the variance of the drag coefficient above the amount expected due to built-in self-correlation.

The observed mean Charnock constant (α in Equation (14)) for RASEX is 0.04 and has a standard deviation of 0.11. The mean value of α is 0.015 for on-shore flow and 0.073 for off-shore flow. The value for on-shore flow is similar to the coastal zone values reported by Garratt (1977) and Wu (1980), 0.017 and 0.018, respectively, and larger than the value of 0.011 reported by Smith (1980, 1988) for the open-ocean. The large dimensionless roughness for off-shore flow reflects the young wave age due to limited fetch conditions in RASEX.

The wave age modified Charnock model (Equation (13)) with $K = 0.48$ and $p = 1$ fits the RASEX data reasonably well, but systematically overpredicts the mean drag coefficient and underpredicts the sensitivity to wave age. A Charnock model of this form with $K = 2.9$ and $p = 2$ best fits the RASEX data. Compared to the HEXOS result, the RASEX drag coefficients are relatively small due to the absence of large amplitude swell and are strongly dependent on wave age.

5. Off-shore Flow Fetch-Dependent Model

For many applications, the wave state is not known. As an alternative simpler approach, we parameterize the 10 m neutral drag coefficient in terms of the dimensionless fetch, F_*, (Perrie and Toulany, 1990; Geernaert and Smith, 1997) as

$$C_{dn} = C_o(1 + a_o \exp(-F_*/F_c)) \tag{16}$$

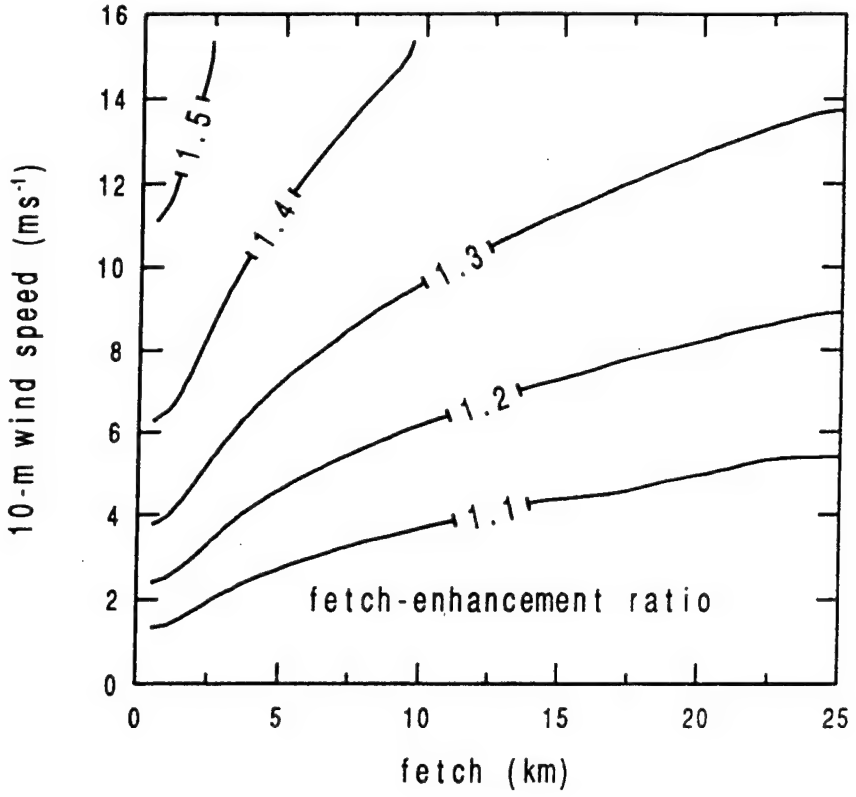

Figure 11. Fetch-enhancement ratio (C_{dn}/C_o) from the fetch dependent model (Equation (16)) as a function of fetch (km) and 10 m wind speed (m s^{-1}).

$$F_* \equiv \left(\frac{gX}{u_*^2}\right)^{1/3}, \tag{17}$$

where X is upwind fetch distance in meters and a_o and F_c are empirical nondimensional parameters based on the RASEX data set. The nondimensional fetch is expected to implicitly include some information on the wave state, which is assumed to be unknown for this application. Recall that shorter fetch off-shore flow is characterized by younger growing waves, larger bandwidth and enhanced drag coefficients compared to longer fetch flow (Figure 3). For the fetch dependent model in this section, we will only consider local off-shore flow, where the dimensional fetch ranges from 2 to 5 km, and the dimensionless fetch F_* ranges from 40 to 150. On-shore flow in RASEX is also fetch limited but is sometimes influenced by wave breaking (Section 3) which may be site specific.

The model (Equation (16)) approaches C_o in the limit of large dimensionless fetch. In this limit, the fetch-enhancement of the drag coefficient vanishes. We assign C_o to be the Charnock prediction for fully developed sea states (Equation (14) with $\alpha = 0.011$).

The parameters $a_o = 0.7$ and $F_c = 100$ in Equation (16) explain 46% of the variance of the observed 10 m neutral drag coefficient in off-shore flow. Constraining

the solution to approach the Charnock prediction in the limit of large dimensionless fetch does not improve the fit but may improve the general applicability of the model. The fetch-enhancement ratio (C_{dn}/C_o in Equation 16) is shown in Figure 11 where the model has been solved iteratively for the friction velocity in fetch-wind speed parameter space. The stability dependent drag coefficient (C_d) could be found by substituting the neutral value (Equation 16) into Equation (5).

6. Conclusions

Observations in shallow water off the Danish coast reveal that, for a given wind speed, the neutral drag coefficient for off-shore flow is larger than for on-shore flow, consistent with the concept of enhanced wind stress over younger growing waves. The drag coefficient increases with wind speed for wind speeds greater than 4 m s^{-1}, and increases with decreasing wind speed for wind speeds less than 4 m s^{-1}. However, wind speed explains only a small fraction of the variance of the neutral drag coefficient which is more strongly related to wave state.

The drag coefficients for off-shore flow in RASEX are relatively large for a given wind speed due to relatively small values of the wave age, and are similar to those reported by Donelan (1982) based on data collected near the coast of Lake Ontario, Canada. *For a given wave age*, the drag coefficients in RASEX are smaller than in most previous open-ocean studies, possibly due to the near absence of large amplitude swell and multiple wave directions.

The Charnock prediction explains only an additional 8% of the variance of the neutral drag coefficient above the amount explained due to self-correlation. For the present data, the smooth flow contribution to the roughness length is unable to adequately predict the increase of the drag coefficient at weak wind speeds. This increase can be included by formulating the drag coefficient in terms of wave age (C_p/u_*).

The strong role of wave age is based primarily on the true age of the wind-driven waves where young growing waves travel more slowly relative to the wind speed and are steeper with greater drag compared to older waves in near-equilibrium with the wind field. However, some of the variance explained by the wave age parameter in this data is related to breaking of large waves with strong on-shore flow. Wave breaking enhances the drag coefficient and corresponds to large high frequency wave height variance, reduced values of the wave phase speed and small values of the wave age parameter.

An attempt to reduce the drag coefficients to their neutral values left significant dependence of the neutral drag coefficient on the stability parameter (z/L) in the most non-neutral cases. This failure may be due to the Charnock assumption in the reduction procedure, the specific form of the stability functions, the importance of additional length scales such as the internal boundary layer depth or large errors in the fluxes and Obukhov length at weak wind speeds.

The neutral drag coefficient has been modelled in terms of wave age (C_p/u_*) and a dimensionless parameter ($B_w\lambda/U$) based on the frequency bandwidth of the wave height spectra (Equation (12)). The frequency bandwidth parameter accounts for the fact that the drag coefficient is greater than the wave age prediction when the wave height spectra are broad due to multiple wave modes. Such broad spectra most often occur with off-shore flow, light winds or following a change of wind direction. The new model successfully predicts the light wind speed regime where the drag coefficient increases with decreasing wind speed. The empirical parameters of the fit and the variance explained by this model are nearly identical when partitioning the data into off and on-shore cases.

A surrogate off-shore flow model is developed for the neutral drag coefficient in terms of dimensionless fetch for application to situations where the wave state is not known. This model approaches the mature wave Charnock prediction in the limit of large dimensionless fetch.

The present study does not include the dependence of the drag coefficient on the angles between the wind, wave and stress vectors (Rieder et al., 1994; Rieder, 1997) nor does it explicitly consider separate contributions from different parts of the wave spectra to the total stress.

Acknowledgements

This work is supported by grant N00014-96-1-0014 from the Office of Naval Research. Jørgen Højstrup is gratefully acknowledged for providing the wave calculations and directing RASEX. Jim Edson, Jim Wilczak and Jeffrey Hare are gratefully acknowledged for their collection of the RASEX data. We also thank Karl Rieder for supplying the open-ocean data, and Jielun Sun, Mark Bourassa, Gary Geernaert, Michel Freilich and the anonymous reviewers for their valuable comments.

References

Alam, A. and Curry, J. A.: 1997, 'Determination of Surface Turbulent Fluxes Over Leads in Arctic Sea Ice', *J. Geophys. Res.*, submitted.

Banner, M. L. and Melville, W. K.: 1976, 'On the Separation of Air Flow Over Water Waves', *J. Fluid Mech.* **77**, 825–842.

Banner, M. L.: 1990, 'The Influence of Wave Breaking on the Surface Pressure Distribution in Wind-Wave Interactions', *J. Fluid Mech.* **211**, 463–495.

Barthelmie, R. J., Courtney, M. S., Højstrup, J., and Sanderhoff, P.: 1994, 'The Vindeby Project: A Description', Report R-741(EN), Risø National Laboratory, DK4000, Roskilde, Denmark.

Charnock, H.: 1955, 'Wind Stress Over a Water Surface', *Quart. J. Roy. Meteorol. Soc.* **81**, 639–640.

Donelan, M. A.: 1982, 'The Dependence of the Aerodynamic Drag Coefficient on Wave Parameters', in *First International Conference on Meteorology and Air-Sea Interaction of the Coastal Zone*, American Meteorological Society, Boston, Mass., pp. 381–387.

Donelan, M. A.: 1990, 'Air–Sea Interaction', in B. LeMehaute and D. M. Hanes (eds.), *Ocean Engineering Science*, John Wiley and Sons, New York, pp. 239–292.

Donelan, M. A., Dobson, F. W., Smith, S. D., and Anderson, R. J.: 1993, 'On the Dependence of Sea Surface Roughness on Wave Development', *J. Phys. Oceanogr.* **23**, 2143–2149.

Fairall, C. W., Bradley, E. F., Rogers, D. P., Edson, J. B., and Young, G. S.: 1996, 'Bulk Parameterization of Air-Sea Fluxes for Tropical Ocean-Global Atmosphere Coupled-Ocean Atmosphere Response Experiment', *J. Geophys. Res.* **101**, 3747–3764.

Freilich, M. H. R. and Guza, R. T.: 1984, 'Nonlinear Effects of Shoaling Surface Gravity Waves', *Phil. Trans. Roy. Soc., London* **A311**, 1–41.

Freilich, M. H. R., Guza, R. T., and Elgar, S. L.: 1990, 'Observations of Nonlinear Effects in Directional Spectra of Shoaling Gravity Waves', *J. Geophys. Res.* **95**, 9645–9656.

Garratt, J. R.: 1977, 'Review of Drag Coefficients over Oceans and Continents', *Mon. Wea. Rev.* **105**, 915–929.

Geernaert, G. L. and Katsaros, K. B.: 1986, 'Incorporation of Stratification Effects on the Oceanic Roughness Length in the Derivation of the Neutral Drag Coefficient', *J. Phys. Oceanogr.* **16**, 1580–1584.

Geernaert, G. L., Katsaros, K. B., and Richter, K.: 1986, 'Variation of the Drag Coefficient and Its Dependence on Sea State', *J. Geophys. Res.* **91**, 7667–7679.

Geernaert, G. L., Larsen, S. E., and Hansen, F.: 1987, 'Measurements of the Wind Stress, Heat Flux and Turbulence Intensity During Storm Conditions over the North Sea', *J. Geophys. Res.* **92**, 127–139.

Geernaert, G. L.: 1988, 'Drag Coefficient Modelling for the the Near Coastal Zone', *Dyn. Atmos. Oceans* **11**, 307–322.

Geernaert, G. L. and Smith, J. A.: 1997, 'On the Fetch and Depth Dependent Drag Coefficient over Coastal and Inland Sea', *Dyn. Atmos. Oceans*, submitted.

Højstrup, J.: 1994, 'Characteristic Wave Periods and Wave Directions', Risø National Laboratory, Roskilde, Denmark.

Højstrup, J., Edson, J., Hare, J., Courtney, M. S., and Sanderhoff, P.: 1997, 'The RASEX 1994 Experiments', Risø -R-788, Risø National Laboratory, Roskilde, Denmark (ISBN-87-550-2039-9), 24 pp.

Kitaigorodskii, S. A.: 1970, 'The Physics of Air-Sea Interaction', translated from Russian, Israel Program for Scientific Translations, Jerusalem, 273 pp.

Large, W. G. and Pond, S.: 1981, 'Open Ocean Momentum Flux Measurements in Moderate to Strong Winds', *J. Phys. Oceanogr.* **11**, 324–336.

Maat, N., Kraan, C., and Oost, W. A.: 1991, 'The Roughness of Wind Waves', *Boundary-Layer Meteorol.* **54**, 89–103.

Mahrt, L., Vickers, D., Howell, J., Højstrup, J., Wilczak, J. A., Edson, J., and Hare, J.: 1996, 'Sea Surface Drag Coefficients in RASEX', *J. Geophys. Res.* **101**, 14,327–14,335.

Nordeng, T. E.: 1991, 'On the Wave Age Dependent Drag Coefficient and Roughness Length at Sea', *J. Geophys. Res.* **96**, 7,167–7,174.

Paulson, C. A.: 1970, 'The Mathematical Representation of Wind Speed and Temperature Profiles in the Unstable Atmospheric Surface Layer', *J. Appl. Meteor.* **9**, 857–861.

Perrie, W. and Toulany, B.: 1990, 'Fetch Relations for Wind-Generated Waves as a Function of Wind-Stress Scaling', *J. Phys. Oceanogr.* **20**, 1666–1681.

Rieder, K. F., Smith, J. A., and Weller, R. A.: 1994, 'Observed Directional Characteristics of the Wind, Wind Stress and Surface Waves on the Open Ocean', *J. Geophys. Res.* **22**, 589–596.

Rieder, K. F.: 1997, 'Analysis of Sea Surface Drag Parameterizations in Open Ocean Conditions', *Boundary-Layer Meteorol.*, submitted.

Schotanus, P., Nieuwstadt, F. T. M., and De Bruin, H. A. R.: 1983, 'Temperature Measurement with a Sonic Anemometer and Its Application to Heat and Moisture Fluxes', *Boundary-Layer Meteorol.* **26**, 81–93.

Sheppard, P. A., Tribble, D. T., and Garratt, J. R.: 1972, 'Studies of Turbulence in the Surface Layer over Water (Lough Neagh), 1, Instrumentation, Programme and Profiles', *Quart. J. Roy. Meteorol. Soc.* **98**, 627–641.

Smedman, A. S., Tjernström, M., and Hogström, U.: 1994, 'Near-Neutral Marine Atmospheric Boundary Layer With No Surface Shearing Stress: A Case Study', *J. Atmos. Sci.* **23**, 3399–3411.

Smith, S. D. and Banke, E. G.: 1975, 'Variation of the Sea Surface Drag Coefficient With Wind Speed', *Quart. J. Roy. Meteorol. Soc.* **101**, 665–673.

Smith, S. D.: 1980, 'Wind Stress and Heat Flux Over the Ocean in Gale Force Winds', *J. Phys. Oceanogr.* **10**, 709–726.

Smith, S. D.: 1988, 'Coefficients for Sea Surface Wind Stress', *J. Geophys. Res.* **93**, 15,467–15,472.

Smith, S. D., Anderson, R. J., Oost, W. A., Kraan, C., Maat, N., DeCosmo, J., Katsaros, K. B., Davidson, K. L., Bumke, K., Hasse, L., and Chadwick, H. M.: 1992, 'Sea Surface Wind Stress and Drag Coefficients: The Hexos Results', *Boundary-Layer Meteorol.* **60**, 109–142.

Snyder, R. L., Dobson, F. W., Elliott, J. A., and Long, R. B.: 1981, 'Array Measurements of Atmospheric Pressure Fluctuations Above Surface Gravity Waves', *J. Fluid Mech.* **102**, 1–59.

Stewart, R. W.: 1974, 'The Air-Sea Momentum Exchange', *Boundary-Layer Meteorol.* **6**, 151–167.

Toba, Y. and Koga, M.: 1986, 'A Parameter Describing Overall Conditions of Wave Breaking, White Capping, Sea-Spray Production and Wind Stress', in E. C. Monahan and G. Mac Niocaill (eds.), *Oceanic Whitecaps*, D. Reidel, Dordrecht, pp. 37–47.

Vickers, D. and Mahrt, L.: 1997, 'Quality Control and Flux Sampling Problems for Tower and Aircraft Data', *J. Atmos. Oceanic Tech.* **14**, 512–526.

Wu, J.: 1980, 'Wind Stress Coefficients Over Sea Surface Near Neutral Conditions – A Revisit', *J. Phys. Oceanogr.* **10**, 727–740.

3. Heat Flux in the Coastal Zone

L. Mahrt and Dean Vickers
College of Oceanic and Atmospheric Sciences, Oregon State University, Corvallis, OR 97331, USA

Jim Edson
Woods Hole Oceanographic Institute
Woods Hole, MA 02543, USA

Jielun Sun
Program in Atmospheric and Oceanic Sciences, University of Colorado, Boulder, CO, 80309, USA

Jørgen Højstrup
Dept. of Meteorology and Wind Energy, Risø National Laboratory, 4000 Roskilde, Denmark

Jeffrey Hare
CIRES, U. of Colorado/NOAA, Boulder, CO 80303 USA

James M. Wilczak
Environmental Technology Lab., ERL/NOAA, Boulder, CO 80303 USA

October 10, 1997

Abstract.

Various difficulties with application of Monin-Obukhov similarity theory are surveyed including the influence of growing waves, advection and internal boundary layer development. Things complications are normally important with offshore flow. The transfer coefficient for heat is computed from eddy correlation data taken at a mast two kilometers off the Danish coast in RASEX. For this coastal zone data, the thermal roughness length shows no well-defined relation to the momentum roughness length or roughness Reynolds number, in contrast to previous theories. The variation of the momentum roughness length is dominated by wave state. In contrast, the thermal roughness length shows significant dependence on wave state only for small values of wave age where the mixing is apparently enhanced by wave breaking. The development of thin internal boundary layers with offshore flow substantially reduces the heat transfer and thermal roughness length but has no obvious influence on momentum roughness length. A new formulation of the thermal roughness length based on the internal boundary layer depth is calibrated to the RASEX data. For the very stable case, the turbulence is mainly detached from the surface and existing formulations do not apply.

As an alternative to adjusting the thermal roughness length, the transfer coefficient is related directly to the stability and the internal boundary layer depth. This avoids specification of roughness lengths resulting from the usual integration of the nondimensional temperature function. The resulting stability function is simpler than previous ones and satisfies free convection similarity theory without introduction of the gustiness factor. The internal boundary layer also influences the moisture transfer coefficient.

Key words: Surface Heat Flux, Sea Surface Fluxes, Marine Boundary Layer, Monin-Obukhov similarity

1. Introduction

Formulations of the heat flux over the sea are difficult to support from observational data because heat fluxes are generally small or driven by horizontal advection of temperature. Advective effects may lead to deviations from Monin-Obukhov similarity theory. In addition, the transfer coefficients may depend on wave state. It is difficult to sort out the various influences on the transfer coefficient. This introductory section surveys various choices which must be made to apply state-of-the-art Monin-Obukhov similarity theory while Section 2 considers influences on surface fluxes not included in Monin-Obukhov similarity theory. Subsequent sections examine the applicability of similarity theory to offshore tower data.

The transfer coefficient, C_H, is defined by the bulk formula

$$\overline{w'\theta'} = C_H \overline{u}[\theta_o - \theta(z)] \tag{1}$$

where z is the observational height, θ_o is the aerodynamic temperature, and $\overline{u}$ is the speed of the vector averaged wind where the coordinate system has been rotated in the direction of the mean wind. The aerodynamic temperature is defined as that temperature extrapolated to the roughness height using Monin-Okukhov similarity theory (Monin and Obukhov, 1954). From Monin-Obukhov similarity theory, the transfer coefficient for heat may be estimated as

$$C_H = [\frac{k}{ln(z/z_o) - \psi_m}][\frac{k}{ln(z/z_{oT}) - \psi_h}] \tag{2}$$

where k is the von Karman constant, z_o and z_{oT} are the roughness lengths for momentum and heat, respectively, and ψ_m and ψ_h are the stability functions for momentum and heat. These functions are historically determined by first fitting the nondimensional profile functions

$$\phi_h(z/L) \equiv \frac{(\partial\overline{\theta}/\partial z)(kzu_*)}{\overline{w'\theta'}(z)} \tag{3}$$

$$\phi_m(z/L) \equiv \frac{(\partial\overline{u}/\partial z)(kz)}{u_*} \tag{4}$$

to dependencies on z/L where L is the Monin-Obukhov length and u_* is the surface friction velocity. The profile functions or universal similarity functions, $\phi_h(z/L)$ and $\phi_m(z/L)$, are vertically integrated to obtain the stability functions ψ_h and ψ_m which are required to evaluate the transfer coefficient (Eq. 2). This vertical integration (Paulson, 1970) requires that the fluxes and the wind direction are approximately

height-independent and requires additional mathematical approximations (Enriquez and Friehe, 1997).

It is somewhat remarkable that the flux-gradient relationship in the surface layer is described by Monin-Obukhov similarity theory under a wide variety of conditions. When valid, the flux- gradient relationship is a function of only z/L. At the same time, there are a number of situations under which the assumptions for Monin-Obukhov similarity are not met, as investigated in this paper. Unfortunately, virtually all models categorically apply Monin-Obukhov similarity theory for all conditions. No practical alternatives exist.

To apply the bulk formula with Monin-Obukhov similarity theory, the following decisions must be made:

1) The friction velocity, u_*, is normally computed from the magnitude of the vector averaged momentum flux although it is occasionally computed from only the momentum flux in the along-wind direction.

2) The mean flow $\overline{u}$ is sometimes replaced with the time average of the instantaneous speed (Section 2.1).

3) The mean flow is sometimes defined in a coordinate system moving with the surface current; that is the current vector is subtracted from the wind vector.

4) When evaluating the flux-gradient relationship from data, the averaging time for the mean flow must be specified so that the perturbation quantities include all of the turbulent motion but none of the mesoscale motion. This specification is sometimes ambiguous particularly in weak wind and nonstationary conditions, as occurs with the RASEX data.

5) One must specify the length of record over which the fluxes are averaged such that the random flux error is reduced to an acceptable magnitude.

The computed transfer coefficients are sensitive to the above choices in weak wind conditions and therefore are ambiguous (Mahrt et al., 1996). The present study uses the total vector averaged stress and the vector averaged wind speed after removing the current. The fluxes are computed based on deviations from a ten minute average and fluxes are averaged over one hour, as is discussed further in Section 3. In addition to the above choices:

6) The aerodynamic temperature must be related to observable temperatures (Section 1.1).

7) The form of the stability functions, ψ_m and ψ_h, must be specified (Section 1.2).

1.1. Aerodynamic temperature

The aerodynamic temperature is here formally defined as the temperature extrapolated downward to the roughness height for momentum using Monin-Obukhov similarity theory although the precise definition varies between studies (Norman and Becker, 1995; Mahrt et al., 1997; Sun et al., 1997). Detailed profiles are not normally available so that the aerodynamic temperature is usually replaced with the surface radiation temperature over land and either the surface radiation temperature or the subsurface water temperature over water. Errors in radiometrically measured skin temperature are not necessarily small compared to the air-sea temperature difference and use of subsurface water temperature measurements must account for cool skin/warm layer effects (Fairall et al., 1996; Esbensen and McPhaden, 1995). The use of skin temperature as the aerodynamic temperature defines the thermal roughness length which is then sometimes referred to as the "radiometric roughness length" (Brutsaert and Sugita, 1992). This roughness length is an empirical coefficient with uncertain physical meaning.

1.2. Stability functions

In contrast to land surfaces, the position of surface roughness elements over the sea (waves) are moving. If Monin-Obukhov similarity theory is valid, then the stability functions should be independent of the surface characteristics which are represented by the roughness length. The stability profile functions have not been directly verified from observations over the sea although a number of formulations have been constructed over land (Högström, 1988). The stability dependence of the transfer coefficients for the present data are reconsidered in Section 5.

1.3. Application to data

Given ψ_h and ψ_m, two approaches can be pursued. In approach I, the thermal roughness length, z_{oT} is "backed out" of Eq. 2 using the observed fluxes and the skin temperature. The computation of the thermal roughness length is not only sensitive to the measurement of the

surface temperature and choice of stability function but also depends on the various assumptions required to derive Eq. 2. Existing models of the heat flux employing a thermal roughness length assume that the thermal roughness length is systematically related to the roughness length for momentum (e.g., Liu et al., 1979; Fairall et al., 1996) which will be explored further in Section 4.

Approach II "reduces" the drag coefficient and transfer coefficients to their neutral values using the stability functions derived over land and then examines the dependence of the neutral value on wave state, wind speed and other parameters. However, the reduction of the transfer coefficient to neutral conditions must impose restrictions on the roughness length such as Charnock's relationship with constant coefficient (Geernaert and Katsaros, 1986: Geernaert, 1990). Smith (1980, Figure 13), Geernaert (1988) and Mahrt et al. (1996) find that the reduction of the drag coefficient to neutral values does not completely remove the influence of stability although it is not clear if the stability functions themselves are the source of the problem.

The neutral value of the transfer coefficient can then be related to external effects such as wave state. Increase of wave slope leads to an increase of surface area and possible disruption of the surface microlayer which would act to increase the total heat flux (Donelan, 1990) and reduce the neutral value of the transfer coefficient. However, increasing wave slope also leads to sheltering which acts to reduce the heat exchange in the lee of the waves and therefore reduce the total heat flux. These two effects cannot be isolated from existing data. Smith (1980), Makin and Mastenbroek (1996) and DeCosmo et al. (1996) find that the transfer coefficient for heat does not increase significantly with wind speed although the scatter is large. In contrast, the drag coefficient increases with wind speed for moderate and strong winds.

The next section examines additional influences on the surface fluxes not included in Monin-Obukhov similarity theory. The behavior of the thermal roughness length is examined in Section 4 using data from the Risø Air Sea Experiment (RASEX) described in Section 3. A new formulation of the transfer coefficient which includes the case of developing internal boundary layers is constructed in Section 5.

2. Deviations from Monin-Obukhov similarity theory

2.1. Vanishing wind speed

Notice that $\overline{u}$ in Eq. 1 is the vector averaged wind. When the speed of the vector averaged wind vanishes, yet nonzero heat flux remains,

the transfer coefficient must approach infinity in contrast to predictions based on the usual Monin-Obukhov similarity theory. Since the bulk aerodynamic approach was constructed with the premise that mixing is at least partly related to turbulence generated by the mean shear, modification is required to include the free convection limit. This limit can be included by either modifying the original stability functions to account for the free convection limit (Louis, 1979) or modifying the velocity scale in Eq. 1 in which case the original derivation of Eq. 2 is no longer formally valid. For the RASEX data, conditions approaching free convection were not observed since the heat flux is maintained by temperature advection. However, the vector averaged wind does occasionally approach very small values in which case some heat flux may still be generated by meandering motions which are eliminated in the vector averaging process.

The velocity scale can be modified by replacing the speed of the vector averaged wind with the average of the instantaneous wind speed. Mahrt and Sun (1995) show that this replacement can be posed in terms of a gustiness factor (Godfrey and Beljaars, 1991) in the velocity scale such that

$$V^2 = \overline{u}^2 + g(\overline{u}^2, u_*, w_*) \tag{5}$$

where V is the time average of the instantaneous wind speed and w_* is the Deardorff free convection velocity scale. This gustiness factor $g(\overline{u}^2, u_*, w_*)$ can be partitioned into three components: 1) small scale surface layer turbulence which presumably obeys Monin-Obukhov similarity theory, 2) boundary layer scale eddies which are influenced by the depth of the boundary layer and 3) mesoscale motions. The use of the time-averaged instantaneous wind speed as the mean flow velocity scale is inconsistent in the sense that the small scale turbulence and the boundary-layer scale eddies contribute to the "mean velocity scale" in Eq. 1 and at the same time contribute to the "turbulent flux". Even though mesoscale motions cannot always be cleanly separated from the boundary-layer eddies, they must be neglected in any attempts to form boundary-layer similarity arguments. Parameterizing the gustiness factor in terms of the free convection velocity scale leads to the form in Beljaars (1995) and Fairall et al. (1996). The gustiness factor can also be introduced as an *ad hoc* correction, without using the time average of the instantaneous wind speed. In this case, the gustiness factor is identified with the large boundary-layer eddies.

2.2. Flux divergence

Generally, heat fluxes over the ocean are small because the air temperature adjusts to the slowly varying sea surface temperature. Exceptions include cases of strong temperature advection where large air-sea temperature differences can be maintained. Strong horizontal advection is most commonly associated with offshore flow in coastal zones although atmospheric temperature advection associated with warm or cold ocean currents and downward transport of cool air from convective cloud systems may lead to significant air-sea temperature differences over the open ocean. In both cases, horizontal advection might cause:

a) deviation of the flux-gradient relationship from that predicted by Monin-Obukhov similarity theory (Eqs. 3-4)

b) violation of the approximation of height-independent flux assumed in the derivation of Eq. 2

The latter condition implies that the flux measured at the observational level may be significantly different from the actual surface value. For offshore flow, the stationary thermodynamic equation can be approximated as

$$\overline{u}\frac{\partial\overline{\theta}}{\partial x} = -\frac{\partial\overline{w'\theta'}}{\partial z} \tag{6}$$

where again the x-coordinate has been rotated into the wind direction. Integrating from the surface ($z = 0$) to the observational height z

$$\overline{w'\theta'}(z) = \overline{w'\theta'}(0) - \int_0^z \overline{u}\frac{\partial\overline{\theta}}{\partial x}dz \tag{7}$$

As a numerical example, consider evaluation of Eq. 7 for $z = 30$ m for the case where the vertically averaged wind speed in the surface layer is 5 m s^{-1} and the vertically averaged horizontal temperature gradient is 0.3 K km^{-1}, which is typical in the RASEX coastal zone with offshore flow (Barthelmie et al., 1996). This temperature advection corresponds to a vertical change of heat flux over a 30 m layer of approximately 0.05 K ms^{-1} which is substantial compared to the heat flux magnitudes observed at the 10 m level. Both cold air advection with upward heat flux and warm air advection with downward heat flux lead to underestimation of the surface heat flux magnitude. In RASEX, corrections to the heat flux using Eq. 7 could only be estimated when the wind was aligned with the tower on the shore and the offshore tower

which occurs for only a small subset of the data. Therefore, general corrections were not made in which case the transfer coefficient for heat may be significantly underestimated for strong advective conditions.

Betts et al., (1990), Frech (1997) and Sun and Mahrt (1994) also found that the flux divergence in the surface layer could be large due to horizontal advection. The surface heat flux is sometimes estimated assuming the heat flux vanishes in the upper part of the boundary layer and linearly extrapolating from the observational layer down to the surface. Donelan (1990) corrects for the decrease of momentum flux between the surface and observational height by assuming bulk similarity conditions for the boundary layer.

Emeis (1995) allows for vertical convergence of the heat flux by replacing the neutral mixing length kz in Eq. 3 with a more complex form of the mixing length which asymptotically matches mixed layer profiles of mixing length above the surface layer. In his case, the vertical flux convergence is associated with nonstationarity due to diurnal heating of the surface layer. This nonstationarity effect is generally negligible in RASEX. The validity of correcting for flux divergence using linear extrapolation, the method in Donelan (1990) or the method of Emeis (1995) all become uncertain in the case of strong advection and were not applied in this study.

2.3. Additional scales

One can postulate four cases of vertical structure with respect to the observational level (Figure 1). In the classical case (case I in Figure 1), the 10 m observational level is above the wave boundary layer but below the influence of the boundary layer depth on local flux-gradient relationship. That is, the 10 m level is within the surface layer where Monin-Obukhov similarity theory applies and the Monin-Obukhov length and height above the surface are the only relevant length scales. Then the nondimensional profile functions can be related to z/L (Eqs. 3- 4).

In the second case, the 10 m level is within the wave boundary layer (Chalikov and Belevich, 1993) where the part of the atmospheric transporting motions are directly induced by the waves and associated perturbation pressure field in the air. In this layer, Monin-Obukhov similarity theory does not describe the local flux-gradient relationship which also depends on the wavelength of the dominant surface wave, λ (Large et al., 1995). Then the profile functions would depend on z/λ as well as z/L (or equivalently z/L and λ/L. Large et al. (1995) suggests that with strong winds, the thickening wave boundary layer may engulf the usual observational levels. As a result, the wind speed in the wave boundary layer is smaller than that predicted by Monin-Obukhov sim-

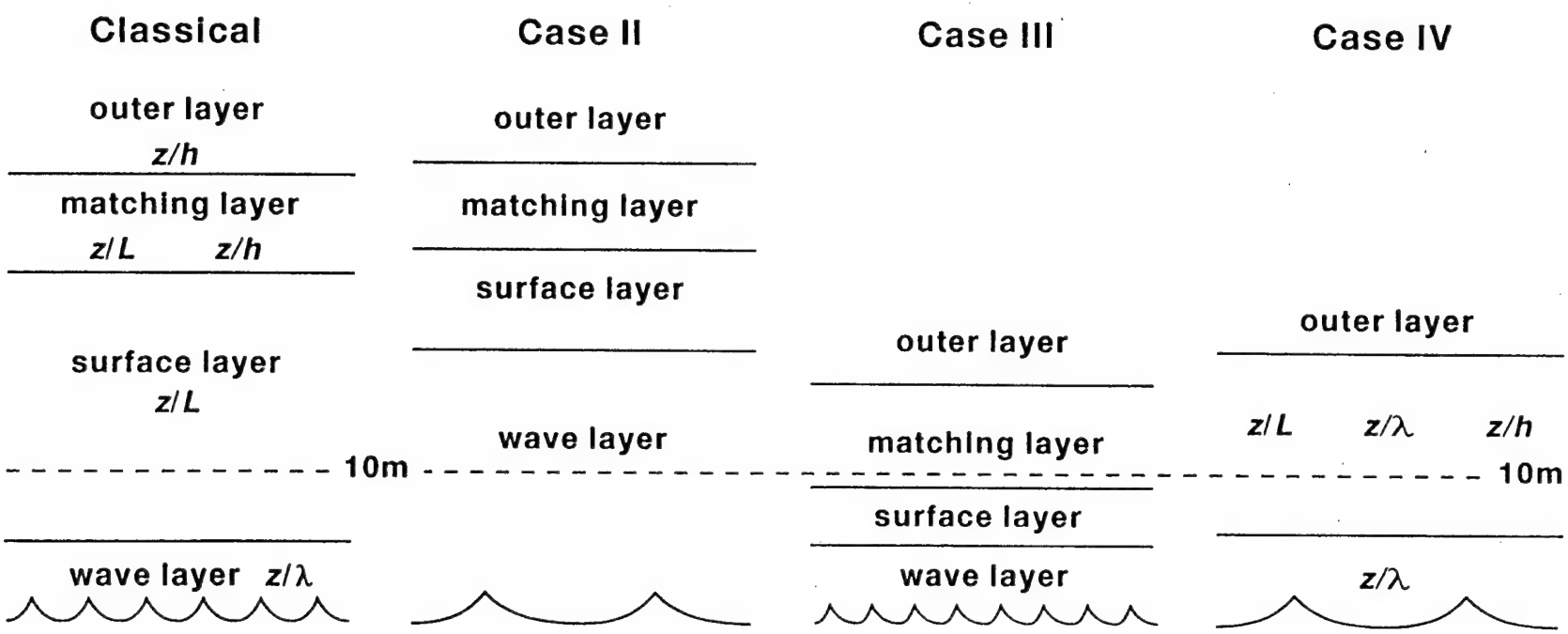

Figure 1. Schematic of different vertical structure with respect to a fixed observational level. Atmospheric similarity relationships are expected to depend on both z/λ and z/L in the wave boundary layer, depend on z/L in the surface layer and depend on both z/L and z/h in the matching layer, where λ is the surface wavelength. In case IV, the matching layer and wave boundary layers overlap and a surface layer satisfying Monin-Obukhov similarity theory does not exist.

ilarity theory which corresponds to a larger drag coefficient for a given stress value. If important, this influence could also lead to increasing transfer coefficient for heat with increasing wind speed. For the RASEX data the wind field at the 3 m level exhibited some coherence with the wave field; however, the wind field at the 6 and 10 m levels did not exhibit such coherence (Hare et al., 1997).

In the third case, the 10 m observational level is above the surface layer in the "matching layer" where the local flux-gradient relationship is influenced by both the Monin-Obukhov length and the boundary layer depth, h. In this case, the heat flux at the observational level may be significantly less than the surface value. This situation appears to be common in the coastal zone as observed in RASEX where developing internal boundary layers are relatively shallow. In the fourth case, a traditional surface layer does not exist at any level as the influence of the boundary layer depth on the flux-gradient relationship extends downward into the wave boundary layer. In this difficult regime, the profile functions would depend on z/h, z/λ and z/L and might even be directly influenced by the Coriolis parameter.

The depth of the internal boundary layer exerts a strong influence on flux-gradient relationship at the 10 m level in RASEX and is considered in more detail in the next subsection.

2.4. Internal boundary layer depth

In cases III and IV, the influence of the internal boundary layer top and entraining motions may extend downward to the observational level. One might generalize the nondimensional temperature gradient to be a function of z/h; that is, $\phi_h(z/L, z/h)$. Grant (1992) suggests that $\phi(z/L)$ for the near neutral boundary layer should be generalized to be of the form $\phi(z/h, h/L, u_*/fh)$ while Khanna and Brasseur (1997) consider the form $\phi(z/L, h/L)$ where ϕ is the nondimensional gradient of an arbitrary variable. In the LES results of Khanna and Brasseur (1997), the nondimensional shear decreases above the surface layer as is also observed by Smedman and Johansson (1997) in shallow offshore boundary layers. Apparently, the vertical gradient decreases more rapidly above the surface as compared to the slower vertical decrease of the flux. No specific formulation for generalization of ϕ to include the dependence on boundary layer depth has been attempted. A simpler approach is pursued in Section 5 where the transfer coefficient is related directly to the stability z/L and the internal boundary layer depth.

In conditions approaching free convection, h/z_o is sometimes considered to be an additional scaling parameter although the physical and

mathematical roles of h/z_o depends on the underlying assumptions (Zilitinkevich et al., 1997). In the treatment of Schumann (1988), the transfer of heat is related to development of internal boundary layers associated with horizontal convergence of boundary layer scale, convectively driven, eddies. The internal boundary layer depth is assigned to be proportional to the boundary layer depth itself. In local free convection (Fairall and Grachev, 1997), a weak dependence on boundary layer depth is introduced through use of the Deardorff convective velocity scale and the transfer coefficient for heat becomes inversely related to the boundary- layer depth.

The depth of the internal boundary layer is generally not available from observations and the initial development of the internal boundary layer is normally poorly resolved in numerical models or difficult to estimate from the modelled vertical structure. In RASEX, the depth of the internal boundary could not be determined for many of the days because the internal boundary layer was deeper than the tower layer or profiles were too noisy. We therefore employ a scaling estimate of the internal boundary layer based on readily available information. This scaling estimate can be formulated by beginning with the simple growth relationship (Højstrup, 1981; Garratt, 1990; Mahrt, 1996 and papers surveyed therein)

$$\partial h_{IBL}/\partial x = C\frac{\sigma_w}{\overline{u}} \tag{8}$$

where h is now equated to the internal boundary layer depth, h_{IBL}, and C is a nondimensional coefficient chosen to be 0.5. The standard deviation of the vertical velocity due to turbulent fluctuations, σ_w, is not normally predicted in numerical models but can be parameterized according to Troen and Mahrt (1986) based on the observations of Højstrup (1982)

$$(\sigma_w)^3 = u_*^3 + a_1 w_*^3 \tag{9}$$

Here, w_* is a "local" free convection velocity scale where the boundary layer depth is replaced by the observation height in the definition of w_* and $a_1 = 2.8$. Assuming constant growth rate, the scale value of the internal boundary layer depth at a downstream fetch of X is estimated by integrating Eq. 8 from the shore ($x = 0$) to X. This leads to the depth scale

$$h_{IBL} = C(u_*^3 + a_1 w_*^3)^{1/3}\ \frac{X}{\overline{u}} \tag{10}$$

Within the simplifications of this development, we expect the observed internal boundary layer depth to be proportional to this scale value. In

offshore cases, it was possible to compare the numerical value of Eq. 10 with the estimated internal boundary-layer depth based on vertical profiles of fluxes using six levels of sonic anemometers in RASEX. In order to reduce noise, the profiles were averaged for different classes of stability. These comparisons indicate that Eq. 10 overestimates the internal boundary-layer depth. The comparison can be improved by assigning a_1 to be 1.0 instead of 2.8 which will be used in Sections 4-5. The overestimation is probably due to the fact that Eq. 10 is only a scaling value which does not account for the general decrease of the growth rate in the downstream direction (Källstrand and Smedman, 1997) and neglects the influence of overlying stratification (Garratt, 1990) and subsidence associated with flow acceleration over the water. In very stable cases, the depth of the internal boundary layer is not definable, as discussed further in Section 3.

In spite of the severe restrictions used to derive Eq. 10, this scaling value explains much of the variation of the transfer coefficient in RASEX (Section 4-5).

3. Data

This study analyzes data collected in fall of 1994 from a research tower in shallow water (4 m) located 2 km off the Danish coast (Barthelmie et al., 1994; Højstrup et al., 1997). The fluctuating wind and virtual temperature data were measured with a Gill/Solent Ultrasonic Anemometer with an asymmetric head mounted approximately 10 m above the sea surface. The asymmetric head was aligned such that the supporting struts did not distort the flow in the preferred wind directions. Tilt corrections are presented in Mahrt et al. (1996). Data for wind directions between 340° and 120° were eliminated due to tower interference and possible interference from wind turbines northeast of the observation tower. The velocity of the current is subtracted from the wind vector although this effect is unimportant except in a few weak wind cases. Average 10 m air temperature was measured with a 100 ohms platinum resistance thermometer (Pt100) constructed at the Risø National Laboratory.

3.1. Fluxes

The time series are divided into one hour subrecords in order to evaluate the random and systematic flux errors. The data set consists of 546 one hour values. Records with large relative random flux sampling errors (> 0.75), large relative systematic error (> 0.75) and large relative

flux events (> 3) (Vickers and Mahrt, 1997a) for heat and momentum fluxes are discarded. As in Mahrt et al., (1996), most of the rejected records are weak wind cases. The reduced data set consists of 436 one hour values of the heat flux. The turbulent perturbations are computed as deviations from 10 minute nonoverlapping averages. The flux is computed by averaging the product of perturbations over a one hour period. Given the flux values and assigning the aerodynamic temperature to be the surface radiation temperature, the roughness lengths are computed using the stability functions of Paulson (1970).

The buoyancy flux is computed using virtual temperature fluctuations approximated from the sonic anemometer after making corrections for bending of the acoustic wave by the crosswind flow. The sensible heat flux was computed from the estimated virtual heat flux by removing the moisture flux term computed from the fast response Ophir moisture sensor mounted at 18 m (Sempraviva and Højstrup, 1997). For 43 of the one hour periods, the Ophir was inoperable and replaced with measurements based on the Väisälä moisture sensor. The slower response time of this instrument appears to lead to some underestimation of the flux which can be tolerated in the calculation of the sensible heat flux in RASEX. The moisture flux contribution to the virtual heat flux is significant only when the sensible heat flux is very small.

The underestimation of the moisture flux by the Väisälä moisture sensor does appear to be important for the moisture flux itself and the calculation of the transfer coefficient for moisture. Only moisture flux values computed from the Ophir can be used for the computation of the transfer coefficient for moisture. This reduces the size of the data set. The dependence of the transfer coefficient for moisture on internal boundary layer depth is similar to that for heat although the scatter is larger. This analysis is not included in this paper.

3.2. Surface temperature

Ideally, one wishes to model the heat flux in terms of the skin temperature rather than the subsurface water temperature since conduction between the water and air is directly coupled to the skin temperature. However, measured skin temperature suffers a number of errors including uncertainty of surface emissivity (dependent on sun angle and wave state) and radiometer calibration errors. Even with calibration, state of the art radiometers are thought to be reliable only within one degree. For typical air-sea temperature differences of a few degrees, a one degree error in the surface radiation temperature can lead to large errors in the transfer coefficient computed from data.

For the RASEX data, the heat flux is strongly correlated to the temperature difference between the air at 10 m and the surface radiation temperature. However, there appears to be an offset in that the heat flux is downward when $T_{sfc} - T_{air} < 1.2\ C°$. Since calibration of the radiometer is not sufficiently accurate and the 10 m air temperature may have calibration errors as well, we adjust the air-sea temperature difference by reducing the surface radiation temperature by 1.2 C°. In other words, the expectation that the heat flux is gradient over the thin layer between 10 m and the surface is considered to be more reliable than the calibration of the radiometer. In previous studies, including Fairall et al. (1996) where the skin temperature was thought to be sufficiently accurate to measure the cool skin effect, countergradient fluxes between the surface and the atmospheric observational level were not reported. In RASEX, the same temperature offset of roughly 1.2 $C°$ occurs in the flux-gradient relationship using the heat flux at the 6 m level. The adjustment of the air-sea temperature difference does not account for time-dependent calibration requirements such as dependence of the radiation reference temperature on wind speed and variable emissivity.

In addition to infra-red measurements, the surface temperature was measured with a Pt100 floating thermometer built at the Risø National Laboratory. The floating thermometer could be affected by absorption of solar radiation and occasional emersion into the air. However, some confidence is placed in the floating thermometer because it correlates with the near bottom (3.5 m) temperature with r=0.96. The average difference between the floating and bottom temperatures is less than 0.1 °C except for weak wind conditions (< 2 m s^{-1}). For significant wind, the difference between two temperatures is small because of wave induced vertical mixing over the shallow depth of the water. The floating and bottom temperatures also show an offset with respect to the relationship between the flux and the air-sea temperature difference. However this offset is smaller, on the order of 0.5°C. If we apply the cool skin correction of Fairall et al. (1996) to the floating temperature, this offset decreases to a few tenths of a degree. In RASEX, the sun angle is low and synoptic conditions are generally windy and cloudy so that the influence of solar radiation on the skin temperature is small compared to the cool skin effect. In fact, the difference between the cool skin corrected surface temperature and the subsurface temperature shows no diurnal variation.

In this study, the transfer coefficients and thermal roughness length will be computed using the air-sea temperature difference based on the surface radiation temperature after the adjustment for the 1.2 °C offset.

4. Roughness length

The usual approach to modelling the heat flux is to equate the aerodynamic temperature with the skin temperature and adjust the corresponding roughness length for heat such that similarity theory predicts the correct heat flux (approach I, Section 1.3). We have computed the thermal roughness length in this manner using the stability functions of Paulson (1970).

For RASEX, this thermal roughness length shows a weak tendency to increase with increasing wind speed and is generally smaller than the momentum roughness length, particularly at weak winds (Figure 2). However, the dependence of thermal roughness length on wind speed shows large scatter and the wind speed explains only 5% of the variance of the thermal roughness length. In contrast to RASEX conditions, DeCosmo et al. (1996) find that the thermal roughness length based on the skin temperature decreases with increasing wind speed although the scatter is also large.

This roughness length for heat is often modeled in terms of the momentum roughness length. For example, applying the model of Liu et al. (1979) to the RASEX values of the roughness Reynolds number, the resulting thermal roughness length increases with increasing momentum roughness length for small values of momentum roughness length and decrease with increasing momentum roughness length for moderate and large values of the momentum roughness length. In contrast, the thermal roughness length in RASEX shows a slight tendency to increase with the momentum roughness length for all values of the momentum roughness length (not shown) although the scatter is too large to construct a definite relationship.

In fact, the two roughness lengths are governed by different physics. The momentum roughness length for this data set is dominated by wave state and independently increases at weak winds (Vickers and Mahrt, 1997b). On the other hand, the thermal roughness length is more related to the occurrence of internal boundary layers and is especially small in weak offshore flow, as discussed below. The expected enhancement of heat flux due to increased momentum roughness length and corresponding stronger turbulence is secondary.

For the coastal zone conditions in RASEX, the internal boundary layer depth scale (Eq. 10) is by far the best predictor of the thermal roughness length (Figure 3) in spite of the crude assumptions invoked in its derivation. The relationship is best defined for unstable cases. For very stable cases, the thermal roughness length becomes large in spite of thin internal boundary layers. In these very stable case, the boundary layer is poorly defined. These cases, which comprise 2% of

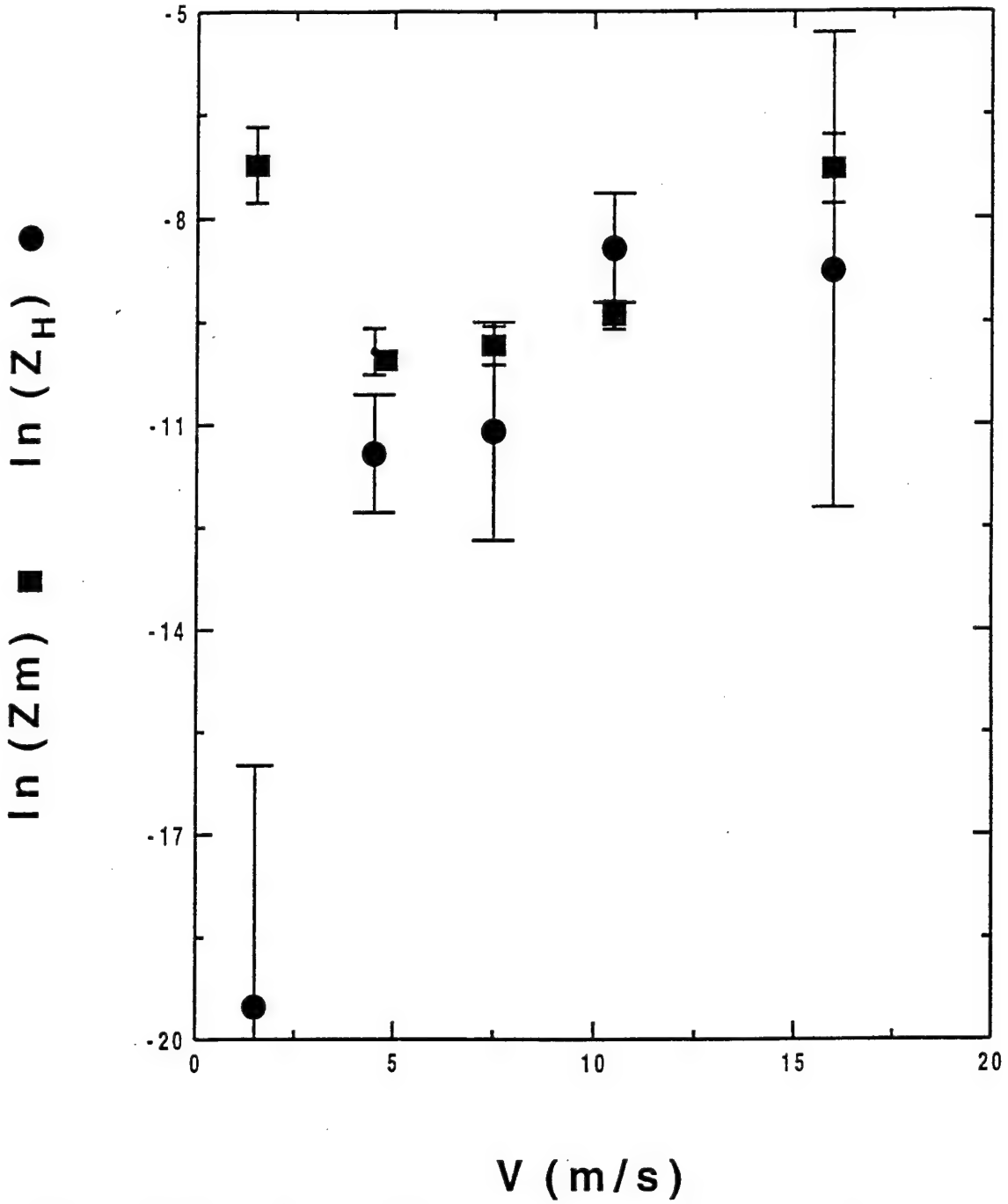

Figure 2. Dependence of the momentum roughness length (squares) and thermal roughness length (circles) on wind speed. The width of each bin on the x- axis is based on the frequency distribution of the variable to ensure an adequate number of variables in each bin. The vertical error bars are the standard error.

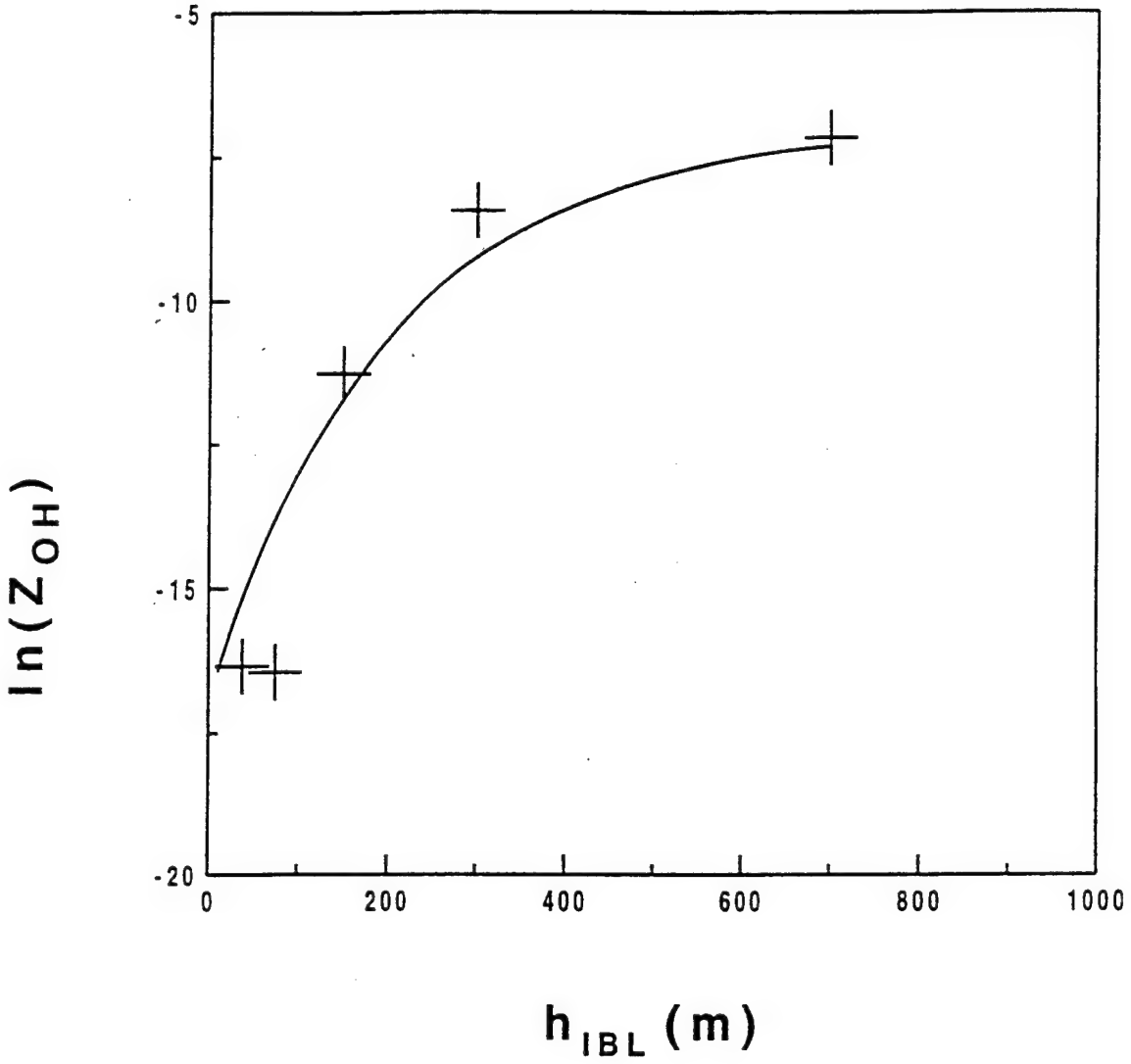

Figure 3. Dependence of the thermal roughness length on the internal boundary layer depth scale (Eq. 10). The solid line is the relationship defined by Eq. 11.

the total data, are omitted from the present analysis and discussed separately at the end of this section.

Small values of the internal boundary-layer depth scale correspond to very small values of the thermal roughness length (Figure 3). In other terms, the transport at 10 m is influenced by the depth of the boundary layer and the assumptions for M-O similarity theory are not met or possibly valid only in a thin layer below the 10 m observational height (Figure 1, case III). The strong dependence of the thermal roughness length on the internal boundary layer depth scale could be potentially due to built in correlation since both the internal boundary layer depth and thermal roughness length are related to the surface heat flux. However, the observed thermal roughness length is also significantly negatively correlated to fetch suggesting that this artificial correlation is not the dominant factor.

The substantial reduction of the thermal roughness length and associated transfer coefficient with thin internal boundary layers could be due to the following related mechanisms:

a) Suppression of large efficient transporting eddies by the low boundary layer top. This effect could explain the substantial reduction of the transfer coefficient in the unstable case. This reduction of the transfer coefficient did not occur in the very stable case where large eddies are not expected. Smedman et al. (1995) suggested that formation of a low level jet at the top of the stable internal boundary layer in offshore flow suppressed the large eddies and reduced the flux relative to the vertical gradient (increased ϕ_h). In RASEX, low level jets were not systematically identified within the tower layer of 45 m, although wind maxima could have occurred above the tower layer.

b) Influence of advective effects on the flux-gradient relationship has not been isolated from data. With offshore advection of cold air, the turbulence may be increasing in the downstream direction due to buoyancy generation of turbulence. This corresponds to advection of weaker turbulence kinetic energy. However, in the absence of substantial cold air advection, the upstream turbulence and surface stress are probably greater due to greater roughness over the land corresponding to advection of stronger turbulence kinetic energy over the sea. The role of advection of turbulence on the flux-gradient relationship for heat is not known.

c) Strong temperature advection can cause substantial vertical divergence of the heat flux in which case the magnitude of the heat flux at 10 m is significantly less than the surface flux. That is, the upward

heat flux decreases with height with cold air advection and downward heat flux increases toward the surface with warm air advection. For the thinnest internal boundary layers in RASEX, the heat flux decreases by as much as 50% between the 3 m and 10 m levels.

d) Dependence of thermal roughness length on stability could be due to inadequacy of the stability functions which is somehow correlated with the internal boundary layer depth. Mahrt and Ek (1993) show that the computed roughness lengths can depend significantly on the choice of the stability function.

In the remainder of this paper, we will refer to the statistical relationship of the thermal roughness length and transfer coefficient to the internal boundary-layer depth scale as the "internal boundary-layer effect". However the cause of this physical dependence may be one or more of the above effects, or effects not yet identified.

The dependence of the thermal roughness length on the internal boundary-layer depth suggests that use of existing similarity theory to predict the heat flux in the coastal zone requires modification to include the influence of the internal boundary-layer depth. One might wish to develop a new formulation of the stability function ϕ_h (Sections 1-2) in terms of both the Monin-Obukhov length and the internal boundary-layer depth. Here, we pursue the simpler approach of retaining the existing stability functions and require the thermal roughness length to absorb of the influence of the boundary-layer depth.

Based on Figure. 3, the thermal roughness length can be formulated as

$$ln(z_{oH}) = ln(z_{oH})_{mod} - 10exp(-\alpha\frac{h_{IBL}}{z}) \qquad (11)$$

where $(z_{oH})_{mod}$ (in meters) is modelled in terms of some existing prediction of the thermal roughness length for long fetch conditions, z is the observational height of 10 m and h_{IBL} is computed from Eq. 10. Based on the present data, $ln(z_{oH})_{mod}$ is chosen to be -7, in which case α is found by visual inspection to be about 0.05. Then the argument of the exponential decay term is $h_{IBL}/200m$. Eq. 11 can not be applied if h_{IBL} becomes smaller than z since the observational level would be above the internal boundary layer. Analogous problems occur in numerical models where z would be the first model level.

The thermal roughness length is not reduced by the internal boundary -layer effect for very stable internal boundary layers where the stratification is isothermal or stronger. It may be that the usual stability functions for Monin-Obukhov similarity theory already underestimate

fluxes for the very stable case (Kondo, 1978; Sun et al., 1997). For example, existing theories do not explicitly include intermittent downward transport of heat by shear generated turbulence above the surface based inversion. This situation is observed in the very stable nocturnal boundary layer over land (Mahrt, 1985; Smedman, 1988: Nappo, 1991). Inclusion of such mixing requires larger values of the thermal roughness length which may offset reduction of the thermal roughness length by the internal boundary layer effect, as modelled by Eq. 11. Indeed, the very stable cases in RASEX include examples where the turbulence and downward heat flux were significant above 30 m but near zero within measurement error at the 10 m level. The assumptions for Monin-Obukhov similarity are not satisfied in these cases. However, these cases are exceptions and for most of the cases of thin internal boundary layers, the thermal roughness length is much smaller than predicted by previous theories.

5. Transfer coefficient

Since the physical meaning of the thermal roughness length is uncertain, it is to some extent no more than a tunable parameter. As an instructional experiment, we short circuit this route and attempt to relate the transfer coefficient directly to the Monin-Obukhov length. This approach avoids approximations required in the integration of the nondimensional temperature gradient to obtain the transfer coefficient for heat (Introduction). Admittedly, the following approach may not be universal and will be calibrated for 10 m observations. The observational analysis below will be framed in terms of the functional dependence

$$C_H = C_H(z/L, ln[z/z_{om}], z/h, C_p/u_*) \tag{12}$$

where h is the depth of the boundary layer which is the internal boundary layer depth for the RASEX data and C_p is the phase speed of the dominant surface waves. While the transfer coefficient for heat is indeed larger with unstable conditions and smaller for stable conditions (Figure 4), much of the variance remains unexplained. By interpolating between the slightly stable and slightly unstable categories, the near neutral value of the transfer coefficient is approximately 1.3×10^{-3}. This is comparable or slightly larger than previous values in the literature (e.g., DeCosmo et al., 1996). The comparison is not rigorous since previous values of the neutral transfer coefficient are mainly determined by reducing the value to neutral conditions. This reduction assumes the Charnock relationship with constant coefficient (Geernaert, 1990) which does not perform well for much of the RASEX data.

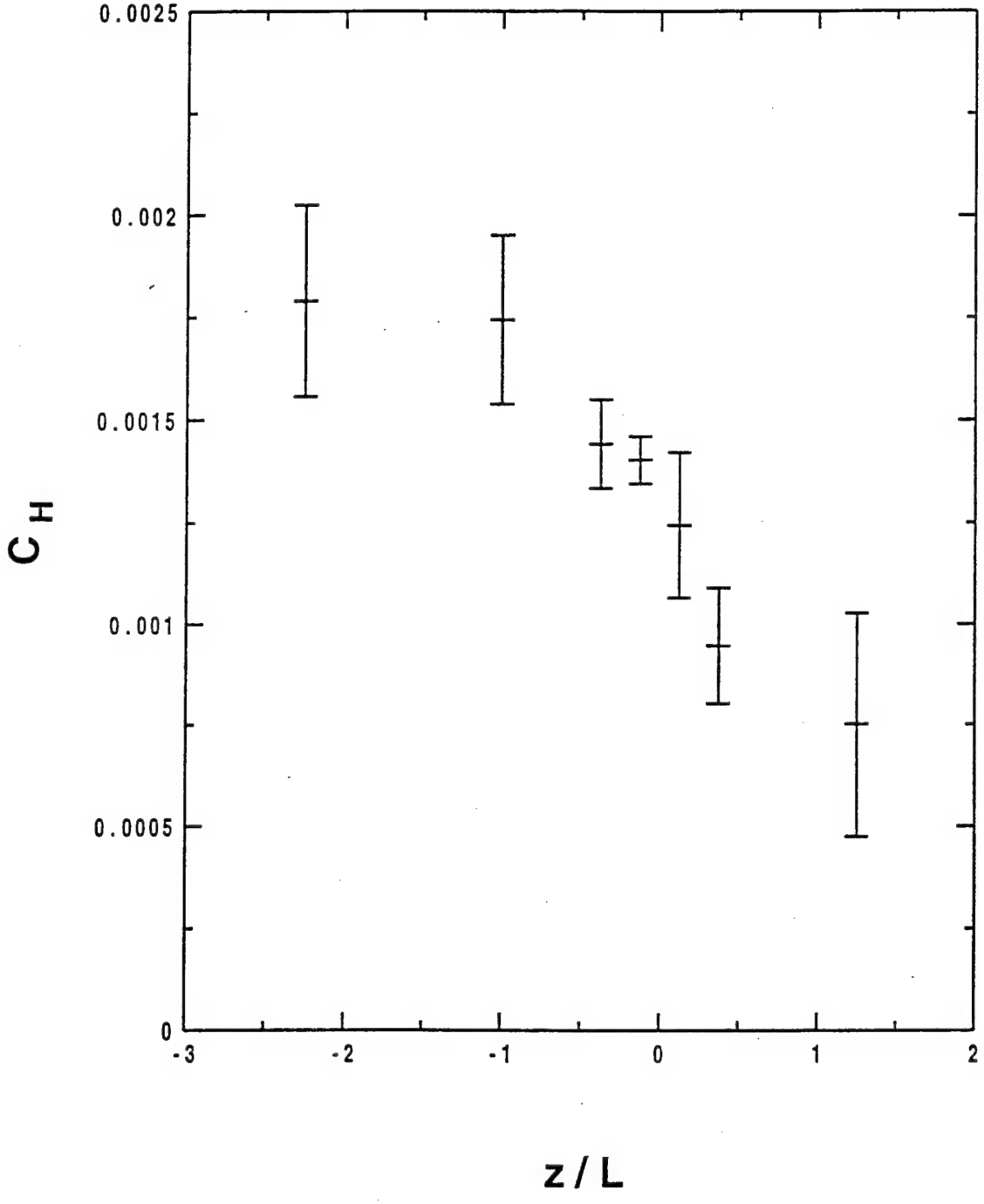

Figure 4. Dependence of the transfer coefficient for heat on stability z/L where z is the 10 m observational height and L is the Monin-Obukhov length.

The transfer coefficient for heat shows a weak tendency to increase with decreasing wave age, C_p/u_* and then shows substantial enhancement for very small values of the wave age (Figure 5). The latter cases occur in strong onshore flow where the small values of wave age are due to slowed phase speed resulting from wave breaking. However the scatter is large. As an aside, this dependency is even smaller for the transfer coefficient defined as $C_t \equiv \overline{w'\theta'}/(u_*[\theta_o - \theta(z)])$ where some of the influence of wave age is presumably included in the variation of the surface friction velocity.

The transfer coefficient for heat shows no significant dependence on the roughness length for momentum suggesting that the increase in heat transfer due to mechanically generated turbulence is already represented in the stability function and linear dependence on wind speed in the bulk formula. Similar conclusions are noted in Donelan (1990). The transfer coefficient for heat shows minimal dependence on wind speed as also observed by Enriquez and Friehe (1997) and others. Consequently, momentum roughness length and wind speed are dismissed as major influences on the transfer coefficient for the data as a whole. For the unstable case, Stull (1994) directly relates the heat flux to the air-surface temperature difference independently of any roughness length. While omission of variations of surface roughness can commit substantial errors in the heat flux when applied to different land surfaces (Sorbjan, 1997), it is a good approximation to the present data.

The transfer coefficient decreases systematically with decreasing depth of the internal boundary layer (Eq. 10) as seen in Figure 6. In terms of linear regression, the internal boundary-layer depth explains 43% of the variance of the transfer coefficient as compared to wave age which explains 8% of the variance of the transfer coefficient. Nonlinear models significantly increase the variance-explained for both variables.

However, some of the dependence on the transfer coefficient on internal boundary-layer depth could be associated with the increase of both the internal boundary-layer depth and the transfer coefficient with instability. We attempt to remove the effect of stability by first fitting the dependence of the transfer coefficient on stability for cases of large internal boundary layer depth where the influence of the depth on the transfer coefficient is assumed to be secondary. Here we use all data points where h_{IBL} is greater than 200 m. A larger cutoff value would be preferable when a larger data set becomes available. For the unstable case with h_{IBL} greater than 200 m, the transfer coefficient can be approximated with the simple function

$$C_H(z/L) = C_{HN} + a(-z/L)^n \tag{13}$$

where C_{HN} is the asymptotic neutral value of the transfer coefficient.

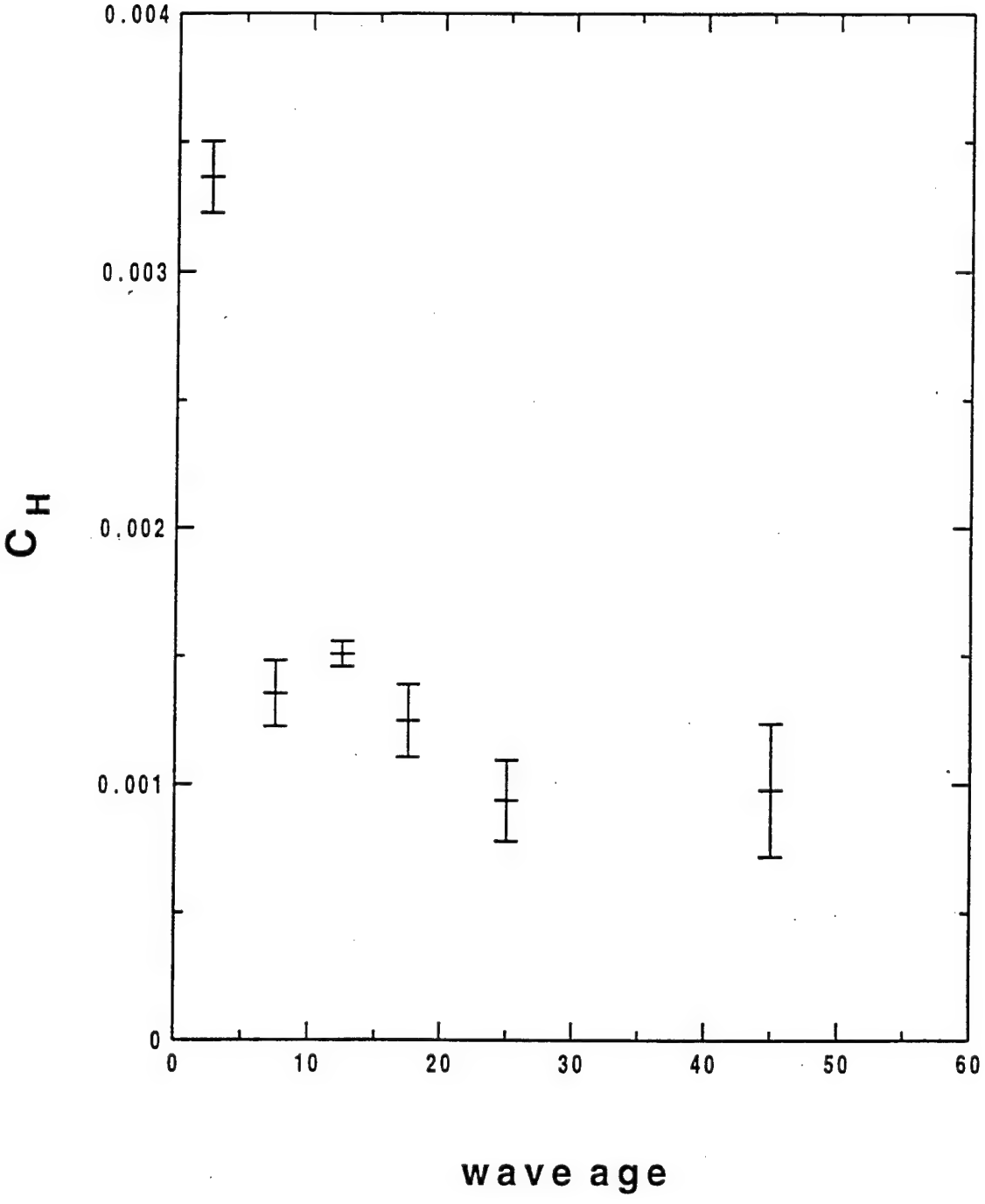

Figure 5. Dependence of the transfer coefficient for heat on wave age.

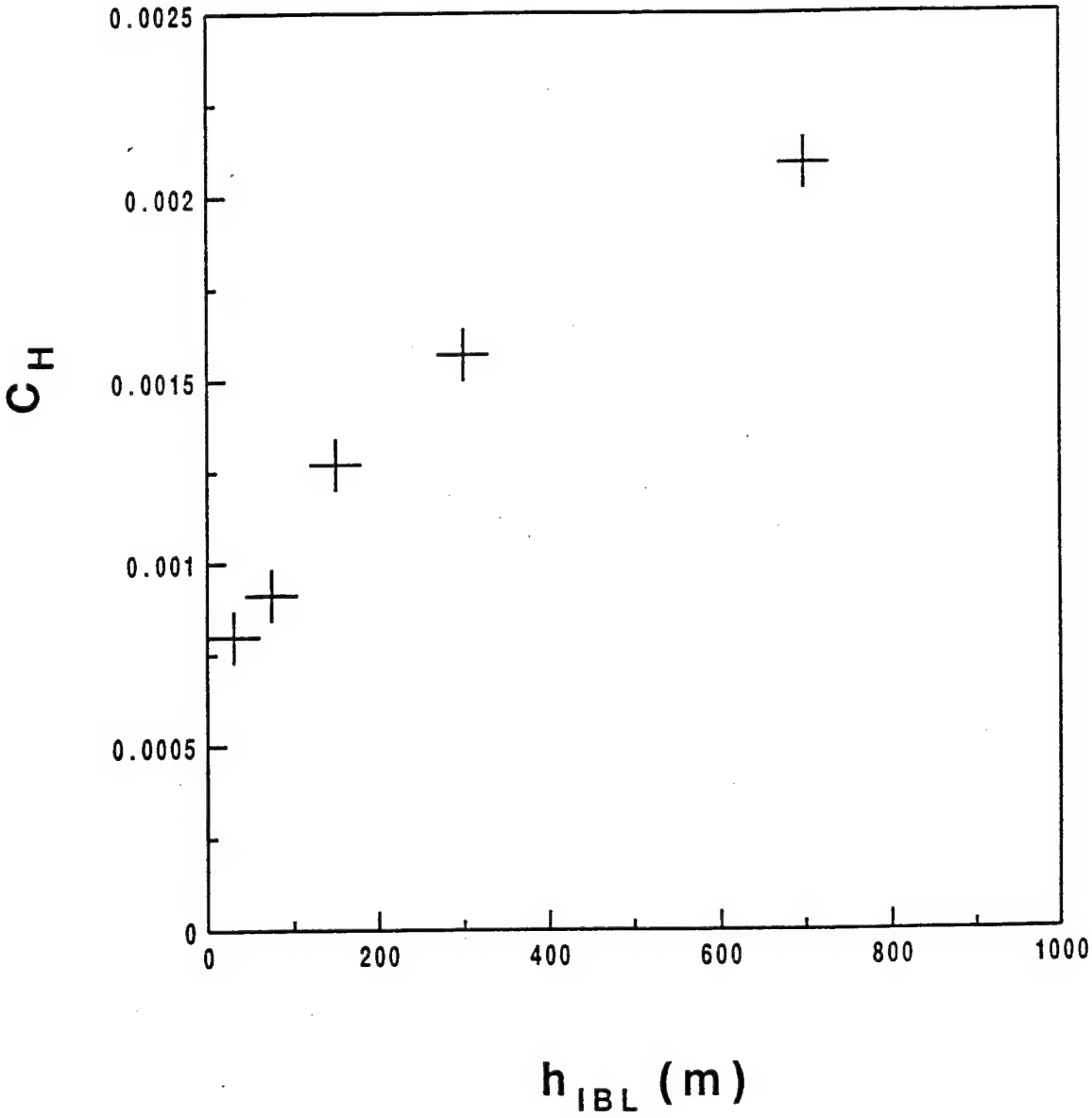

Figure 6. Dependence of the transfer coefficient for heat on the internal boundary-layer depth scale (Eq. 10).

The exponent "n" will be determined by requiring that the turbulent conductance $C_H\ \overline{u}$ does not vanish in the limit of vanishing wind speed. Noting that $u_* = C_D^{1/2}\ \overline{u}$, we can write the conductance in the limit of vanishing mean wind and nonzero heat flux as

$$(-z/L)^n \overline{u} => [\frac{(\kappa g/\Theta)\overline{w'\theta'}z}{C_D^{3/2}\overline{u}^3}]^n \overline{u} \tag{14}$$

where Θ is the basic state potential temperature. Nonvanishing $C_H\ \overline{u}$ with vanishing wind speed requires that $n = 1/3$ which is analogous to the free convection relationship for ϕ_m (e.g., Sorbjan, 1989). The one third power dependence is also used in the stable case since the heat flux may still remain nonzero with vanishing $\overline{u}$ due to the influence of shear generation of turbulence by meandering motions not included in the vector averaged wind. Then Eq. 13 becomes

$$C_H(z/L) = C_{HN} + a(-z/L)^{1/3} \tag{15}$$

Within the large scatter of the data, a reasonable fit for the unstable case for h_{IBL} greater than 200 m is C_{HN}= 1.3 $\times$ 10^{-3} and a = 4.8 x 10^{-4}. Within the large scatter of the data, an adequate fit for the stable case is $a = 8.5\times\ 10^{-4}$.

The residual of the transfer coefficient, not explained by Eq. 15, is not significantly correlated with the stability function z/L for the data as a whole although a more complex stability function could explain slightly more of the variance. Part of the large scatter is due to flux sampling problems, particularly for stable conditions. The random flux error, systematic error and the flux nonstationarity (Vickers and Mahrt, 1997a) tend to be large for the very stable cases ($z/L > 0.5$) even though the cases with the largest errors have already been removed (Section 3). Large sampling errors generally correspond to values of C_H which are smaller than that predicted by Eq. 15, perhaps due to underestimated fluxes. However, the total number of cases for strong stability is small and no additional cases are discarded here.

To study the dependence of the transfer coefficient on effects other than stability, we define the residual transfer coefficient (C_{HR}) which is the deviation of the observed value, C_H, from the value predicted by Eq. 15 ($C_H(z/L)$), such that

$$C_{HR} = C_H - C_H(z/L) \tag{16}$$

While much of the residual transfer coefficient could be due to flux sampling errors, the residual transfer coefficient shows the expected near zero average for h_{IBL} greater than a few hundred meters and

becomes significant negative for small values of h_{IBL} (Figure 7). The residual transfer coefficient shows only weak dependence on wave age similar to that of the original transfer coefficient (Figure 5) and shows no definite dependence on wind speed or momentum roughness length.

The prediction of the transfer coefficient can be substantially improved by modifying Eq, 15 with a dependence on the internal boundary layer depth scale. A good approximation to the data (Figure 7) is

$$C_H = C_H(z/L) - 0.6 \times 10^{-3} exp[\frac{-0.05 h_{IBL}}{z}] \qquad (17)$$

where $C_H(z/L)$ is computed from Eq. 15. This modified transfer coefficient (Eq. 17) approaches the original predicted value, $C_H(z/L)$ as h_{IBL} becomes large compared to 200 m. While application of Eq. 17 is a substantial improvement upon previous approaches, the data was not adequate to cleanly separate out the effects of stability and the internal boundary layer depth. A larger data set with longer fetches is required and more cases with small wave age are needed to document the apparent enhancement of the transfer coefficient with wave breaking.

6. Conclusions

For the coastal zone data collected during RASEX, the thermal roughness length was computed from the observed heat flux, skin temperature and traditional Monin-Obukhov stability functions. The thermal roughness length shows no clear relation to the momentum roughness length or roughness Reynolds number in contrast to previous formulations of the thermal roughness length. The momentum roughness length is strongly influenced by wave state while the thermal roughness length shows only a weak dependence on wave state except for small wave age. The thermal roughness length and transfer coefficient decrease to small values in thin internal boundary layers which occur with short fetches over the water. The present data indicates that the internal boundary layer effect is more significant for unstable conditions compared to stable conditions. Suppression of large efficient transporting eddies by the low boundary layer top is one of several plausible explanations of the reduced heat flux (Section 4). In addition, the heat flux at the 10 m observation level is significantly less than the surface value for thin internal boundary layers. A larger more complete data set is required to better estimate the internal boundary-layer depth and separate the roles of internal boundary-layer depth, stability and wave state.

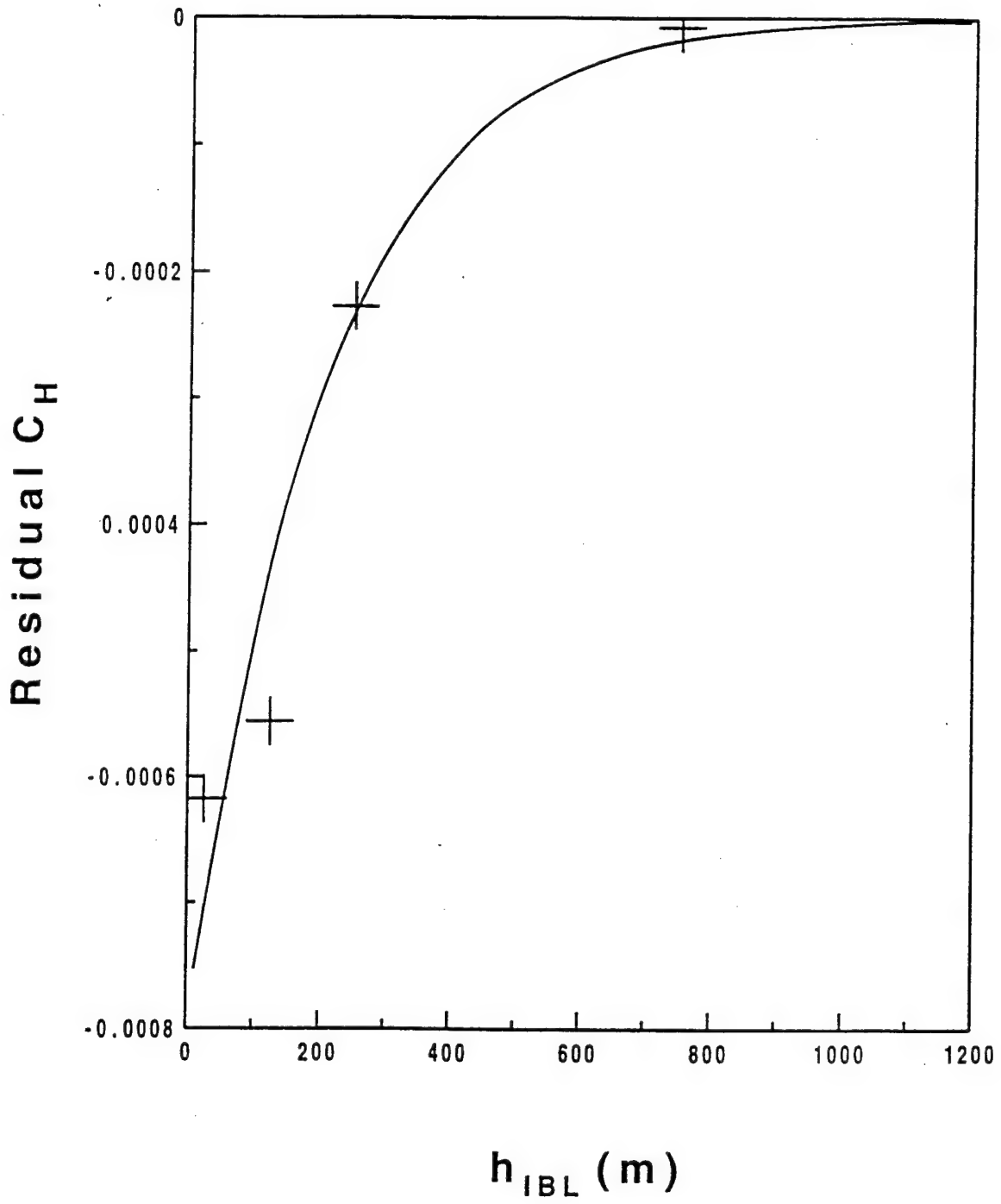

Figure 7. Dependence of the residual transfer coefficient for heat on the internal boundary-layer depth scale (Eq. 10). The solid line is relationship (Eq. 17).

A new formulation of the thermal roughness based on the internal boundary layer depth scale is calibrated to the RASEX data (Section 4). The corresponding transfer coefficient then depends on both the Obukhov length through the stability functions and internal boundary layer depth through the thermal roughness length. This approach was chosen instead of generalizing the Monin-Obukhov stability function (ϕ_h) to include the internal boundary layer depth since the latter approach combines two independent physical effects into one function and is more demanding in terms of data requirements. The relationship between the thermal roughness length and the internal boundary layer depth breaks down in the very stable case where the boundary layer is characterized by an upside down structure with the generation of turbulence occurring mainly detached from the surface.

As an alternative approach, the transfer coefficient is also formulated directly in terms of stability without requiring use of the roughness lengths (Section 5). This formulation of the transfer coefficient includes the factor of two reduction in thin internal boundary layers. Although the moisture flux measurements appeared to be not as reliable, the transfer coefficient for moisture exhibited the same dependence on the internal boundary layer depth as that for heat except with larger scatter (not shown in this study).

Further improvement of similarity theory would benefit from more accurate measurements of sea surface temperature. If one questions applicability of the existing stability functions derived over land, a larger data set is required to sort out the effects of stability, wave state, vertical flux divergence and internal boundary-layer depth.

Acknowledgements

This work is supported by grant N00014-1-96-0014 from the Office of Naval Research. The comments of the two reviewers are greatly appreciated.

References

Barthelmie, R. J., Courtney, M. S., Højstrup, J., and Sanderhoff, P.: 1994, 'The Vindeby Project: A Description', Report R-741(EN), Risø National Laboratory, DK4000, Roskilde, Denmark.

Barthelmie, R. J., Grisogono, B., and Pryor, S. C.: 1996, 'Observations and Simulations of Diurnal Cycles of Near-Surface Wind Speeds Over Land and Sea', *J. Geophys. Res.* **101**, 21,327-21,337.

Beljaars, A. C.: 1995, 'The Parametrization of Surface Fluxes in Large Scale Models Under Free Convection', *Quart. J. Roy. Met. Soc.* **121**, 255-270.

Betts, A. K., Desjardins, R. L., MacPherson, J. I., and Kelly, R. D.: 1990, 'Boundary-Layer Heat and Moisture Budgets from FIFE'. *Boundary-Layer Meteorol.* **50**, 109-138.

Brutsaert, W. H., and Sugita, M.: 1992, 'Regional Surface Fluxes From Satellite-Derived Surface Temperatures (AVHRR) and Radiosonde Profiles', *Boundary-Layer Meteorol.* **58**, 355-366.

Chalikov, D. V., and Belevich, M. Y.: 1993, 'One-Dimensional Theory of the Wave Boundary Layer' *Boundary-Layer Meteorol.*, **63**, 65-96.

DeCosmo, J., Katsaros, K. B., Smith, S. D., Anderson, R. J., Oost, W. A., Bumke, K., and Chadwick, H.: 1996, 'Air-Sea Exchange of Water Vapor and Sensible Heat: The Humidity Exchange Over the Sea (HEXOS) Results', *J. Geophys. Res.* **101**, 12,001-12,016.

Donelan, M.: 1990 'Air-Sea Interaction', *Ocean Engineering Science*, B. LeMehaute and D. M. Hanes, Eds. John Wiley and Sons, 239-291.

Emeis, S.: 1995, 'Determination of the Surface Sensible Heat Flux from Aircraft Measurements', *Beit. Phys. Atmos.* **68**, 143-148.

Enriquez, A. G. and Friehe, C. A.: 1997, 'Bulk Parameterization of Momentum, Heat, and Moisture Fluxes Over a Coastal Upwelling Area', To appear in *J. Geophys. Res.*.

Esbensen, S. K., and McPhaden, M. J.: 1995, 'Enhancement of Tropical Ocean Evaporation by Atmospheric Mesoscale Systems', *Journal of Clim.* **9**, 2307-2325.

Fairall, C. W., Bradley, E. F., Rogers, D. P., Edson, J. B., and Young, G. S.: 1996, 'Bulk Parameterization of Air-Sea Fluxes for Tropical Ocean-Global Atmosphere Coupled-Ocean Atmosphere Response Experiment', *J. Geophys. Res.* **101**, 3747-3764.

Fairall, C. W., and Grachev, A. A.: 1997, 'Air-Sea Fluxes and Sea Surface Roughness Length in the Free Convection Limit', Submitted to *J. Atmos. Sci.*.

Frech, M.: 1997, 'The Mesoscale Moisture Variability and its Impact on the Energy Transfer through the Boundary Layer', Submitted to *Boundary-Layer Meteorol.*.

Garratt, J. R.: 1990, 'The Internal Boundary Layer - A Review', *Boundary-Layer Meteorol.* **50**, 171-203.

Geernaert, G. L. and Katsaros, K. B.: 1986, 'Incorporation of Stratification Effects on the Oceanic Roughness Length in the Derivation of the Neutral Drag Coefficient', *J. Phy. Oc.*, **16**, 1580-1584.

Geernaert, G. L: 1988, 'Influence of Coastal Fetch-Limited Waves on Determining the Wind Stress During Diabatic Conditions', *Ninth Symposium on Turbulence and Diffusion*, Roskilde, Denmark, Amer. Met. Soc., 54-57.

Geernaert, G. L.: 1990, 'Bulk Parameterizations for the Wind Stress and Heat Fluxes', *Surface Waves and Fluxes. Vol. 1 - Current Theory*, 91-172, G. L. Geernaert and W. J. Plant, Eds., Kluwer.

Godfrey, J. S., and Beljaars, A. C. M.: 1991, 'On the Turbulent Fluxes of Buoyancy, Heat and Moisture at the Air-Sea Interface at Low Wind Speeds', *J. Geophys. Res.* **96**, 22,043 -22,048.

Grant, A. L. M.: 1992, 'The Structure of Turbulence in the Near-Neutral Atmospheric Boundary Layer', *J. Atmos. Sci.* **49**, 226-239.

Hare, J. E., Hara, T., Edson, J. B., and Wilczak, J. M.: 1997, 'A Similarity Analysis of the Structure of Airflow Over Surface Waves', To appear in *J. Phy. Oc.*.

Högström, U.: 1988, 'Non-Dimensional Wind and Temperature Profiles in the Atmospheric Surface Layer: A Re-evaluation', *Boundary-Layer Meteorol.* **42**, 55-78.

Højstrup, J.: 1981, 'A Simple Model for the Adjustment of Velocity Spectra in Unstable Conditions Downstream of an Abrupt Change in Roughness and Heat Flux', *Boundary-Layer Meteorol.* **21**, 341-356.

Højstrup, J.: 1982, 'Velocity Spectra in the Unstable Planetary Boundary Layer', *J. Atmos. Sci.*,**39**, 2239-2248.

Højstrup, J., Edson, J., Hare, J., Courtney, M. S., Sanderhoff, P.: 1997, 'The RASEX 1994 Experiments', *Risø -R-788, (ISBN-87-550-2039-9)*, 24 pp, Risø National Laboratory, Roskilde, Denmark.

Khanna, S. and Brasseur, J. G.: 1997, 'Analysis of Monin-Obukhov Similarity from Large Eddy Simulation', To appear in *J. Fluid Mech.*.

Kondo, J., Kanechika, O., and Yasuda, N.: 1978, 'Heat and Momentum Transfer Under Strong Stability in the Atmospheric Surface Layer', *J. Atmos. Sci.* **35**, 1012-1021.

Källstrand, B. and Smedman, A.-S.: 1997, 'A Case Study of the Near-Neutral Coastal Internal Boundary-Layer Growth: Aircraft Measurements Compared with Different Model Estimates', *Boundary-Layer Meteorol.* **85**, 1-33.

Large, W. G., Morzel, J., and Crawford, G. B.:1995, 'Accounting for Surface Wave Distortion of the Marine Wind Profile in Low-Level Ocean Storms Wind Measurements', *J. Phy. Oc.* **25**, 2959-2971.

Liu, W. T., Katsaros, K. B., Businger, J. A., and Tillman, J. E.: 1979, 'Heat Transport and Thermal Structure in the Interfacial Boundary Layer Measured in an Open Track of Water in Turbulent Free Convection', *J. Atmos. Sci.* **36**, 1722-1735.

Louis, J.-F.: 1979, 'A Parametric Model of Vertical Eddy Fluxes in the Atmosphere', *Boundary-Layer Meteorol.* **17**, 187-202.

Mahrt, L.: 1985, 'Vertical Structure and Turbulence in the Very Stable Boundary Layer', *J. Atmos. Sci.* **42**, 2333-2349.

Mahrt, L.: 1996, 'The Bulk Aerodynamic Formulation Over Heterogeneous Surfaces', *Boundary-Layer Meteorol.* **78**, 87-119.

Mahrt, L., and Ek, M.: 1993, 'Spatial Variability of Turbulent Fluxes and Roughness Lengths in HAPEX-MOBILHY', *Boundary-Layer Meteorol.* **65**, 381-400.

Mahrt, L., and Sun, J.: 1995, 'The Subgrid Velocity Scale in the Bulk Aerodynamic Relationship for Spatially Averaged Scalar Fluxes', *Mon. Wea. Rev.* **123**, 3032-3041.

Mahrt, L., Vickers, D., Howell, J., Edson, J., Hare, J., Højstrup, J., and Wilczak, J.: 1996, 'Sea Surface Drag Coefficients in RASEX', *J. Geo. Res., Oceans* **101**, 14,327-14,335.

Mahrt, L., Sun, J., MacPherson, J. I., Jensen, N. O., Desjardins, R. L.: 1997, 'Formulation of the Surface Temperature for Prediction of Heat Flux: Application to BOREAS', To appear in *J. Geophy. Res.*.

Makin, V. K. and Mastenbroek, C.: 1996, 'Impact of Waves on Air-Sea Exchange of Sensible Heat and Momentum', *Boundary-Layer Meteorol.* **79**, 279-300.

Monin, A. S. and Obukhov, A. M.: 1954, 'Basic Laws of Turbulent Mixing in the Ground Layer of the Atmosphere', *Trudy Geofiz. Inst. Akad. Nauk SSSR* **151**, 163-187.

Nappo, C. J.: 1991, 'Sporadic Breakdown of Stability in the PBL Over Simple and Complex Terrain', *Bound.-Layer Meteor.* **54**, 69-87.

Norman, J. M., and Becker, F.: 1995, 'Terminology in Thermal Infrared Remote Sensing of Natural Surfaces', *Agric. and For. Met.* **77**, 153-166.

Paulson, C. A.: 1970, 'The Mathematical Representation of Wind Speed and Temperature Profiles in the Unstable Atmospheric Surface Layer', *J. Appl. Meteor.* **9**, 857-861.

Sempraviva, A.-M. and Højstrup, J.: 1997, 'Temperature and Humidity Variance and Covariance Budget in the Marine Surface Layer', Submitted to *Boundary-Layer Meteorol.*.

Schumann, U.: 1988, 'Minimum Friction Velocity and Heat Transfer in the Rough Surface Layer of a Convective Boundary Layer', *Bound. Lay. Meteor.* **44**. 311-326.

Smedman, A.-S.: 1988, 'Observations of a Multi-Level Turbulence Structure in a Very Stable Atmospheric Boundary Layer', *Boundary-Layer Meteorol.* **44**, 231-253.

Smedman, A-S, Bergström, H., and Högström, U.: 1995, 'Spectra, Variances and Length Scales in a Marine Stable Boundary Layer Dominated by a Low Level Jet', *Boundary-Layer Meteorol.* **76**, 211-232.

Smedman, A.-S., and Johansson, C.: 1997, 'Modifications of Monin-Obukhov Similarity Theory in Unstable Conditions', *12th Symposium on Boundary Layers and Turbulence.* Amer. Met. Soc., Vancouver, 273-274.

Smith, S. D.: 1980, 'Wind Stress and Heat Flux Over the Ocean in Gale Force Winds', *J. Phy. Oc.* **10**, 709-726.

Sorbjan, Z.: 1989, 'Structure of the Atmospheric Boundary Layer', Prentice Hall, Englewood Cliffs, NJ, USA, 317 pp.

Sorbjan, Z.: 1997, 'Comments on "A Convective Transport Theory for Surface Fluxes', *J. Atmos. Sci.* **54**, 576-578.

Stull, R. B.: 1994, 'A Convective Transport Theory for Surface Fluxes', *J. Atmos. Sci.* **51**, 3-22.

Sun, J., and Mahrt, L.: 1994, 'Spatial Distribution of Surface Fluxes Estimated from Remotely Sensed Variables', *J. Appl. Meteor.* **33**, 1341-1353.

Sun, J., Massman, W., and Grantz, D.: 1997, 'Aerodynamic Variables in the Bulk Formula', Submitted to *Boundary-Layer Meteorol.*.

Troen, I. and Mahrt, L: 1986, 'A Simple Model of the Atmospheric Boundary Layer: Sensitivity to Surface Evaporation', *Boundary-Layer Meteorol.* **37**, 129-148.

Vickers, D. and Mahrt, L.: 1997a, 'Quality Control and Flux Sampling Problems for Tower and Aircraft Data', To appear *J. Atm. and Oc. Tech.*.

Vickers, D. and Mahrt, L.: 1997b, 'Fetch Limited Drag Coefficients over Shallow Water', To appear in *Boundary-Layer Meteorol.*.

Zilitinkevich, S., Grachev, A., and Hunt, J. C. R.: 1997, 'Non-Local Heat and Mass Transfer in the Shear-Free Convective Surface Layer', Submitted to *J. Fluid Mech.*.

Figure Legends

Figure 1. Schematic of different vertical structure with respect to a fixed observational level. Atmospheric similarity relationships are expected to depend on both z/λ and z/L in the wave boundary layer, depend on z/L in the surface layer and depend on both z/L and z/h in the matching layer, where λ is the surface wavelength. In case IV, the matching layer and wave boundary layers overlap and a surface layer satisfying Monin-Obukhov similarity theory does not exist.

Figure 2. Dependence of the momentum roughness length (squares) and thermal roughness length (circles) on wind speed. The width of each bin on the x- axis is based on the frequency distribution of the variable to ensure an adequate number of variables in each bin. The vertical error bars are the standard error.

Figure 3. Dependence of the thermal roughness length on the internal boundary layer depth scale (Eq. 10). The solid line is the relationship defined by Eq. 11.

Figure 4. Dependence of the transfer coefficient for heat on stability z/L where z is the 10 m observational height and L is the Monin-Obukhov length.

Figure 5. Dependence of the transfer coefficient for heat on wave age.

Figure 6. Dependence of the transfer coefficient for heat on the internal boundary-layer depth scale (Eq. 10).

Figure 7. Dependence of the residual transfer coefficient for heat on the internal boundary-layer depth scale (Eq. 10). The solid line is relationship (Eq. 17).

4. Universal profile functions

We have completed preliminary work on the behavior of the universal profile functions which is the heart of Monin-Obukhov similarity theory and one of the principal goals of RASEX. *It must be emphasized that these results are tentative and more work is required before definite conclusions can offered.*

The principal conclusions are that:

1. The profile function for momentum, ϕ_m is larger than predicted by Monin-Obukhov similarity theory for unstable offshore flow. This means that the momentum flux is *less* than predicted by the observed gradient and similarity theory. The suppression of the flux could be due to the elimination of the large, efficient, transporting eddies by the shallow top of the internal boundary layer. This is borne out by stress cospectra which show reduced transport at the largest scales compared to onshore flow. The transport by small scale eddies is approximately the same for offshore flow as for onshore flow.

2. The nondimensional temperature gradient ϕ_h shows substantial departure from existing similarity theory only for the case of offshore stable flow where ϕ_h is larger than expected. This departure is possibly due to downward heat flux from shear-generated turbulence at higher levels.

5. Other studies

Michael Frech has analyzed the wave wire data in some detail. He has found numerous problems with the data but still is of the opinion that the data is yielding useful results. A manuscript on these results should be forthcoming but is not available at the writing of this report.

This grant also funded Jørgen Højstrup to reprocess and provide us with additional data from RASEX outside the intensive observational period. Jørgen Højstrup has also carried out a number of assessment studies including flow distortion, calibration studies and instrument intercomparison. Some of these studies are accessible through our RASEX home page http://mist.ats.orst.edu/rasex.

At the writing of this report, H. K. Johnson, H. J. Vested, J. Højstrup, S. E. Larsen and H. Hersbach are revising a manuscript accepted for *Journal of Physical Oceanography* entitled "On the dependence of sea surface roughness on wind waves". This paper acknowledges my ONR grant which was a minor source of funding for this work.

The final report has not included conferences proceedings since all of the material in these proceedings were eventually included in publications in refereed journals. One exception is "Wind-wave modelling in waters with restricted fetches" by Kofoed Hansen, H. K. Johnson, J. Højstrup and J. Lange, *Fifth International Workshop on Wave Hindcasting and Forecasting*, 27-30 January 1998, Melbourne.